

## A relativistic particle pusher for ultra-strong electromagnetic fields

Jérôme Pétri

Université de Strasbourg, CNRS, Observatoire astronomique de Strasbourg, UMR 7550, F-67000 Strasbourg, France.

---

### ARTICLE INFO

Article history:

elsarticle.cls, L<sup>A</sup>T<sub>E</sub>X, Elsevier,  
template 2010 MSC: 00-01, 99-00

---

### ABSTRACT

Kinetic plasma simulations are nowadays commonly used to study a wealth of non-linear behaviours and properties in laboratory and space plasmas. In particular, in high-energy physics and astrophysics, the plasma usually evolves in ultra-strong electromagnetic fields produced by intense laser beams for the former or by rotating compact objects such as neutron stars and black holes for the latter. In ultra-strong electromagnetic fields, the gyro-period is several orders of magnitude smaller than the timescale on which we desire to investigate the plasma evolution. Some approximations are required like for instance artificially decreasing the electromagnetic field strength which is certainly not satisfactory. The main flaw of this downscaling is that it cannot reproduce single particle acceleration to ultra-relativistic speeds with Lorentz factor above  $\gamma \approx 10^3 - 10^4$ . In this paper, we design a new algorithm able to catch particle motion and acceleration to Lorentz factor up to  $10^{15}$  or even higher by using Lorentz boosts to special frames where electric and magnetic fields are parallel. Assuming that these fields are locally uniform, we solve analytically the equation of motion in a tiny region smaller than the length scale of the gradient of the field. This analytical integration of the orbit severely reduces the constrain on the time step, allowing us to use very large time steps, avoiding to resolved the ultra high frequency gyromotion. We performed simulations in ultra-strong spatially and time dependent electromagnetic fields, showing that our particle pusher is able to follow accurately the exact analytical solution for very long times. This property is crucial to properly capture lepton electrodynamics in electromagnetic waves produced by fast rotating neutron stars.

© 2019 Elsevier Inc. All rights reserved.

---

### 1. Introduction

With the advent of numerical simulation techniques and increasing computational power capabilities, plasma physics has benefited from a better and deeper description of its behaviour and properties in many contexts of laboratory experiments and space plasmas. Nowadays numerical simulations play a key role in the development of our knowledges about plasma physics. However, these kinetic simulations still suffers from limits exerted by hardware capabilities. For instance, the Vlasov-Maxwell equations require 3 dimensions in space as well as 3 dimensions in

velocity thus a total 6 dimensions, forbidding us to perform high resolution simulations. Another limitation comes from the different time and space scales to be resolved in order to properly catch the collective plasma effects. The simulation box is usually much larger than the gyro-radius or than the skin depth. Another restriction of particular interest in high-energy physics and astrophysics is the motion of plasmas in ultra-strong magnetic fields. By ultra-strong we mean field strengths about the quantum critical value of  $B \approx 4,4 \cdot 10^9$  T. Such fields are commonly met in neutron star magnetospheres like pulsars (Ptri, 2016) and magnetars (Mereghetti et al., 2015). For pulsars, the magnetic field strength is typically  $B \approx 10^8$  T whereas for magnetars it easily exceeds  $B \approx 10^{10}$  T. These values put stringent constraints on the time step of any numerical algorithm because the gyration period is orders of magnitude smaller than the macroscopic evolution period given by the neutron star rotation frequency  $\Omega = 2\pi/P$  with  $P$  its period of revolution. Indeed, the ratio between the Larmor frequency and the stellar rotation frequency is

$$\frac{\omega_B}{\Omega} = \frac{qB}{m\Omega} = 2,8 \cdot 10^{18} \left( \frac{P}{1 \text{ s}} \right) \left( \frac{B}{10^8 \text{ T}} \right). \quad (1)$$

$B$  is the stellar magnetic field strength,  $\Omega$  its angular velocity,  $q$  the particle charge and  $m$  its mass. For the above numerical applications, we assumed electrons or positrons to be the main constituents of the magnetospheric plasma. Moreover, the Larmor radius associated to these fields is

$$r_L = \frac{\gamma mc}{qB} = 1,7 \cdot 10^{-5} \text{ m} \left( \frac{\gamma}{10^6} \right) \left( \frac{B}{10^8 \text{ T}} \right)^{-1}. \quad (2)$$

$c$  is the speed of light and  $\gamma$  the particle Lorentz factor. This length scale remains much smaller than the typical size of a neutron star estimated to be about  $R_{\text{ns}} = 10$  km. Thus the ratio between Larmor radius and neutron star radius is about  $\epsilon = r_L/R_{\text{ns}} = 10^{-10}$ , allowing to separate both scales. Note that  $R_{\text{ns}}$  is also the typical length scale for the electromagnetic field gradient. To a very good approximation, we can assert that leptons orbiting in this field feel an almost constant and uniform electromagnetic field during thousands to millions of gyro periods.

Particle orbits in a plane electromagnetic wave are described by a one parameter family solution given by the so called strength parameter defined by

$$a = \frac{qE}{mc\omega} \quad (3)$$

$m$  and  $q$  are the particle mass and charge respectively,  $E$  is the amplitude of the wave electric field and  $\omega$  its frequency. This strength parameter is ridiculously small for visible light  $a_{\text{light}} \approx 10^{-10}$ , but substantial for high intensity laser  $a_{\text{laser}} \approx 10^2$  and dramatically high at the surface of neutron stars  $a_{\text{ns}} \approx 10^{18}$ .

Many kinetic codes have been designed to solve the pulsar magnetosphere problem. Unfortunately, none of the PIC results presented so far have been able to put realistic electromagnetic fields into the simulation box (Belyaev, 2015; Philippov and Spitkovsky, 2014; Cerutti et al., 2015). This questions the veracity of those works that even add radiation reaction in a regime not corresponding to what is expected in neutron stars (Cerutti et al., 2016). Some scaling technique is proposed to extrapolate simulation results to realistic values (Kalapotharakos et al., 2018) but such assertions must be checked by direct numerical computations in physically self-consistent fields.

Recently, Zenitani and Umeda (2018) improved the standard Boris particle pusher by computing the exact analytical rotation in the magnetic part of the Lorentz force. They showed an improvement in the accuracy. The Boris algorithm is popular because it is simple and accurate. Its stability is accounted for by its phase space volume preserving properties as shown by Qin et al. (2013). Umeda (2018) proposed an improvement of Boris algorithm by employing a three stage step. Relativistic simulations are even more stringent about numerical error accumulation and volume preserving schemes are highly recommended by Zhang et al. (2015). However, these recent papers did not address the problem of particle pusher in very strong electromagnetic fields.

Efficient particle pushers in ultra-strong electromagnetic fields are nevertheless a fundamental prerequisite to simulate the true electrodynamics in neutron star magnetospheres such as pulsars and magnetars. Specific algorithms have been designed for motion in strong magnetic fields to solve for kinetic plasma problems via numerical simulations. For instance a Vlasov-Poisson approach was tackled by Crouseilles et al. (2017) to solve motion in a strong and uniform external magnetic field using a two-scale formalism. The high frequency gyration about the magnetic field is decoupled from the secular evolution occurring on a much longer time scale. Semi-implicit scheme preserving the asymptotic limit of the guiding centre approximation were also investigated by Filbet and Rodrigues (2015). Geiser and Riedel (2016) discussed the merit of several integrators used in electromagnetic PIC simulations, like the explicit and implicit Boris algorithm and a cyclotronic integrator. An explicit time-reversible cyclotronic integrator has been

derived in Patacchini and Hutchinson (2009) to avoid a fine resolution of the Larmor frequency on some field configurations. Velocity Verlet algorithms for strong homogeneous static external magnetic fields in the context of molecular dynamics have been investigated by Spreiter and Walter (1999) performing a Taylor expansion. For a comprehensive comparison of relativistic particle integrators, see Ripperda et al. (2017). These authors carefully compared the merit of the standard Boris algorithm Boris (1970), the Vay (2008) implicit scheme in space velocity, the Higuera and Cary (2017) second order method and the implicit midpoint method described in Lapenta and Markidis (2011). This leapfrog scheme already appeared in Verboncoeur (2005). A fully implicit update in space and velocity parameters for relativistic particle integrators relying on Vay (2008) velocity advance has been explored by Ptri (2017). There it has been shown that catching properly and accurately the simple electric drift motion in an ultra relativistic regime remains extremely difficult to achieve. Unfortunately, neutron star magnetospheres are common places for such relativistic drift velocities. It is therefore compulsory to design efficient and accurate numerical schemes to faithfully follow these trajectories. This is a crucial step towards realistic particle acceleration and radiation in ultra-strong electromagnetic fields. Some tests of particle acceleration in a plane electromagnetic wave using standard pushers and reported by Arefiev et al. (2015) show severe limitations in the accuracy already for modest strength parameters not above  $a \approx 20$ . This is unacceptable for our investigation of neutron star magnetospheres.

Moreover, when accelerated to very high energies in the high fields of neutron stars, particles are subject to radiation reaction, a stringent friction damping the motion by limiting the Lorentz factor to  $10^8$  or  $10^9$  according to current wisdom. Unfortunately, there is no unique model for implementing this damping into a numerical code. Vranic et al. (2016) proposed a careful study of several radiation reaction forces to be used in classical PIC codes. They showed that all prescriptions for this force give similar results. For pulsars, radiation reaction is inescapable for several reason. First, pulsars are known to be very efficient particle accelerators, pushing pairs to Lorentz factors as high as  $\gamma \approx 10^9$ . See for instance the simulations performed in vacuum by Ptri (2019) assuming radiation reaction force operates in balance with the accelerating electric field. Without radiation reaction, particles would tend to much high Lorentz factors (Finkbeiner et al., 1989). Second, pulsars are also famous for being high energy emitters, producing photons with energy above the GeV even up to TeV ranges for the Crab pulsar (Ansoldi et al., 2016). Therefore radiation inevitably has to impact on the particle dynamics in a non perturbative way. Implementing this additional radiative force into our code is under progress. One approach would be to find exact analytical solutions for constant electromagnetic fields including radiation reaction. Some analytical solutions exist in special cases, for instance in a transverse electromagnetic wave (Hadad et al., 2010). A second approach consist to find an approximate analytical expression for the change in velocity and Lorentz factor during an integration time step for the Lorentz force solely and then correct for radiation reaction (which should remain weak compared to the Lorentz force). The third brute force approach would resolve the full motion including the radiation reaction but at the expense of requiring much smaller time steps. All these options are currently investigated and tested and will be shown in another work.

As particle simulation codes are prone to discrete particle noise scaling as  $1/\sqrt{N_{\text{par}}}$  where  $N_{\text{par}}$  is the number of particles used in the simulation box, a large number of particles is necessary to achieve low level noise results. High performance computing optimizing memory usage and CPU time is recommended (Bowers et al., 2008). However, in this paper we rather focus on achieving very high accuracy in the numerical solution sticking as close as possible to the analytical solutions of the physical problem. Therefore, in this study, computational time is not an issue but setting realistic ultra-strong electromagnetic fields is a stringent and critical issue to be able to properly capture the correct physics. Actually, having not such a severe restriction on the time step compared to other algorithms, the computational extra cost is largely compensated by taking time steps that are thousands to millions or billions of time larger than those required by explicit time integrators. We also expect that GPGPUs will speed up the extra cost of performing the analytical computations of the solutions.

In this paper, we first expose the general idea, detailing the method and the algorithm in section 2. Then we remind the exact analytical solutions for a charged particle in an arbitrary electromagnetic field in section 3 and show how to switch to a frame where  $E$  and  $B$  are parallel. We then test our implementation of these equations in several configurations for which exact analytical solutions are known, see section 5. We conclude about our achievements and possible extensions in section 6.

## 2. General method and algorithm

Our main goal in this paper is to use exact analytical expressions for the particle trajectories in a homogeneous and uniform electromagnetic field. As such expressions are known and very handy in a frame where the electric field  $\mathbf{E}$

and magnetic field  $\mathbf{B}$  are parallel, we introduce two important frames to perform our numerical simulations. First, we denote by  $K$  the observer frame in which we want to evolve the particle motion one time step. Second, we consider a new frame  $K'$  where the electric field and magnetic field are parallel. We will demonstrate that there always exist one such frame. The only exception is when  $E = cB$  and  $\mathbf{E} \cdot \mathbf{B} = 0$  corresponding to a plane electromagnetic wave propagating in vacuum. An excellent and very detailed reference on this topic is Gourgoulhon (2010), but see also Sengupta (2007).

Kinematic and dynamical quantities like position and velocity are transformed according to the special relativistic Lorentz transform valid for any four vector  $\mathbb{A}$ . In our notations, the temporal components are labelled with index 0 whereas the spatial components are labelled with indices running from 1 to 3. The Minkowskian metric is given by the diagonal matrix  $\eta_{ik} = \text{diag}(+1, -1, -1, -1)$ . In particular, the contravariant components  $A^i = (A^0, \mathbf{A})$  of this four vector  $\mathbb{A}$  in both frames are related by

$$A'^0 = \Gamma(A^0 - \mathbf{A} \cdot \mathbf{V}/c) \quad (4a)$$

$$A'_{\parallel} = \Gamma(A_{\parallel} - VA_0/c) \quad (4b)$$

$$\mathbf{A}'_{\perp} = \mathbf{A}_{\perp}. \quad (4c)$$

$A_{\parallel}$  and  $A'_{\parallel}$  are the components along the relative velocity between both frames,  $A_{\perp}$  and  $A'_{\perp}$  the components perpendicular to this relative velocity,  $\mathbf{V}$  is the 3-velocity vector of the frame  $K'$  with respect to the frame  $K$  and  $\Gamma = (1 - V^2/c^2)^{-1/2}$  the associated Lorentz factor. In the following sections, we specialize the basis vectors such that the  $z$  and  $z'$  axis are aligned along  $\mathbf{V}$ . Note that the particle proper frame is never used, only its proper time is required to compute the trajectories.

The procedure to advance the particle position and velocity one time step is then the following. Compute both relativistic electromagnetic invariants  $\mathcal{I}_1 = E^2 - c^2 B^2$  and  $\mathcal{I}_2 = \mathbf{E} \cdot \mathbf{B}$ . If  $\mathcal{I}_2 = 0$  and  $\mathcal{I}_1 \neq 0$ , then a frame where either the electric field or the magnetic field vanishes exists, depending on the sign of  $\mathcal{I}_1$ . We switch to this new frame  $K'$  and solve analytically the equation of motion. If  $\mathcal{I}_1 = 0$ , we have to solve the motion separately as no physical frame  $K'$  exist with speed strictly less than  $c$  where  $\mathbf{E}$  and  $\mathbf{B}$  are parallel. This special case is called a null or light like field. If on the other side  $\mathcal{I}_2 \neq 0$ , there always exists a frame  $K'$  where  $\mathbf{E}$  and  $\mathbf{B}$  are parallel. Then if possible switch to the new frame  $K'$  by a Lorentz boost. Solve the particle motion in  $K'$  and then Lorentz boost back to  $K$ . In the frame  $K'$ , if the  $z'$  axis is not aligned with the common direction of  $\mathbf{E}$  and  $\mathbf{B}$ , we also apply an Euler rotation to bring the new  $z''$  axis along this direction.

To summarize all the cases, we show a pseudo-code explaining how to evolve the particle trajectory depending on the field configuration in table 1. The next step requires the solution of the 4-velocity and 4-position in the frame where  $\mathbf{E}$  and  $\mathbf{B}$  are parallel.

### 3. Charge in an uniform electromagnetic field

In this section, we derive the exact analytical solution of a charged particle in relativistic motion in an uniform electromagnetic field for an arbitrary geometric configuration. To do this we first find a frame where electric  $\mathbf{E}$  and magnetic  $\mathbf{B}$  fields are parallel. Next we solve exactly and analytically the equation of motion in the relativistic regime where the electric field and the magnetic field are parallel. These solutions are also presented in Gourgoulhon (2010) and in Jackson (2001) in a somewhat different way with different integration constants.

A direct integration of the equation of motion in the observer frame needs to solve for the eigenvalues and eigenvectors of the antisymmetric electromagnetic tensor  $F^{ik}$ . This has been performed by Vandervoort (1960) but we found it easier to first switch to the special frame where  $\mathbf{E}$  and  $\mathbf{B}$  are parallel and then compute the solution. This is also the strategy we adopt in our numerical implementation of the algorithm. It is therefore also necessary to readjust the axes to conform to the orientation we employ in the subsequent paragraphs.

#### 3.1. Frame where $\mathbf{E}$ and $\mathbf{B}$ are parallel

A useful way to follow particle trajectories in any prescribed electromagnetic field given in an inertial frame  $K$  consists to Lorentz transform the electromagnetic field into a special frame  $K'$  in which the electric field is parallel to the magnetic field. In the general case, there is an infinite number of frames for which the electric field is parallel to

---

**Algorithm 1:** The algorithm to solve for particle motion.

---

**Input:** The initial 4-position and 4-velocity of the particle  $(x^n, u^n)$  at time  $t^n$ .  
 The electromagnetic invariants  $I_1 = E^2 - c^2 B^2$  and  $I_2 = \mathbf{E} \cdot \mathbf{B}$ .  
**Output:** The final 4-position and 4-velocity of the particle  $(x^{n+1}, u^{n+1})$  at time  $t^{n+1}$ .  
**Data:** Electromagnetic field  $(\mathbf{E}, \mathbf{B})$  at particle position  $x^n$ .

```

/* Check for zero electromagnetic field  $E == B == 0$  */
1 if ( $E == 0 \ \& \ B == 0$ ) then
2   | Integrate particle trajectory according to eq. (38), no update in velocity.
   /* Check for light-like wave  $I_1 == 0 \ \& \ I_2 == 0$  */
3 else if ( $I_1 == 0 \ \& \ I_2 == 0$ ) then
4   | Integrate particle trajectory according to eq. (34), (35)
   /* Check for zero magnetic field  $B == 0$  */
5 else if ( $B == 0$ ) then
6   | Integrate particle trajectory according to eq. (23), (24)
   /* Check for zero electric field  $E == 0$  */
7 else if ( $E == 0$ ) then
8   | Integrate particle trajectory according to eq. (25), (26)
   /* Otherwise integrate in frame where  $\mathbf{E}$  and  $\mathbf{B}$  are parallel */
9 else
10  | Integrate particle trajectory according to eq. (21), (22)
    
```

---

**Table 1.** Pseudo-code summarizing the full algorithm. It shows the many special cases to evaluate and handle (light-like fields, orthogonal fields, arbitrary fields).

the magnetic field. We can however choose the particular velocity given by  $\mathbf{V}_{\parallel} = c \boldsymbol{\beta}_{\parallel} = \alpha \mathbf{E} \wedge \mathbf{B}$  where  $\alpha$  is a constant to be determined. The normalized velocity  $\boldsymbol{\beta}_{\parallel}$  required by the Lorentz transform to get this condition must satisfy

$$\frac{\boldsymbol{\beta}_{\parallel}}{1 + \boldsymbol{\beta}_{\parallel}^2} = \frac{c \mathbf{E} \wedge \mathbf{B}}{E^2 + c^2 B^2} \quad (5)$$

neglecting all other curvature, gradient and polarization drifts in the limit of vanishing Larmor radius which is acceptable in a neutron star ultra-strong magnetic field. Let us denote by a prime quantities expressed in the frame  $K'$  moving at velocity  $\mathbf{V}_{\parallel}$  with respect to  $K$ .

In the frame  $K'$ , the motion is along the common direction of  $\mathbf{E}'$  and  $\mathbf{B}'$  that is the electromagnetic field as measured in this frame  $K'$ . To get the useful solution, we write  $\mathbf{V}_{\parallel} = \alpha \mathbf{E} \wedge \mathbf{B}$ . The constant  $\alpha$  is the solution given by

$$\alpha = \frac{E^2 + c^2 B^2 - \sqrt{I_1^2 + 4 c^2 I_2^2}}{2 (\mathbf{E} \wedge \mathbf{B})^2}. \quad (6)$$

The minus sign in front of the square root enforces a speed less than that of light. The electric and magnetic fields in the frame moving at speed  $\mathbf{V}_{\parallel}$  are found by a special relativistic Lorentz boost of the electromagnetic field and gives

$$\mathbf{E}' = \Gamma_{\parallel} [(1 - \alpha B^2) \mathbf{E} + \alpha (\mathbf{E} \cdot \mathbf{B}) \mathbf{B}] \quad (7a)$$

$$\mathbf{B}' = \Gamma_{\parallel} [(1 - \alpha E^2/c^2) \mathbf{B} + \alpha (\mathbf{E} \cdot \mathbf{B}) \mathbf{E}/c^2]. \quad (7b)$$

The Lorentz factor of the frame in which  $\mathbf{E}'$  and  $\mathbf{B}'$  are parallel is defined by  $\Gamma_{\parallel} = (1 - \boldsymbol{\beta}_{\parallel}^2)^{-1/2}$ . In this frame, the particle trajectory is decomposed into a motion along the common direction of  $\mathbf{E}'$  and  $\mathbf{B}'$  and a gyration around the magnetic field  $\mathbf{B}'$ . Thus the local tangent to the trajectory becomes  $\mathbf{t}'_{\parallel} = \pm \mathbf{E}'/E' = \pm \mathbf{B}'/B'$ , the sign being chosen such that particles flow outwards. Our expression for the particle velocity resembles to the Aristotelian expression given by Gruzinov (2013). Our velocity prescription is however more general because we do not assume that particles travel exactly at the speed of light. The speed along the common  $\mathbf{E}$  and  $\mathbf{B}$  direction is constrained by the electric field

acceleration along  $\mathbf{B}$  contrary to Aristotelian electrodynamics. Gruzinov (2013) introduced two new quantities  $E_0 > 0$  and  $B_0$  according to the following invariants

$$E^2 - B^2 = E_0^2 - B_0^2 \quad (8a)$$

$$\mathbf{E} \cdot \mathbf{B} = E_0 B_0. \quad (8b)$$

Solving for the magnetic field strength  $B_0$ , we get

$$c^2 B_0^4 + I_1 B_0^2 - I_2^2 = 0 \quad (9)$$

and by keeping only the real solution with a positive sign +

$$B_0^2 = \frac{-I_1 + \sqrt{I_1^2 + 4c^2 I_2^2}}{2c^2}. \quad (10)$$

In such a way, plugging this expression into the electromagnetic field transform given in eq. (7) we find

$$\mathbf{E}' = \frac{\Gamma E_0}{E_0^2/c^2 + B^2} \left[ \frac{E_0}{c^2} \mathbf{E} + B_0 \mathbf{B} \right] \quad (11a)$$

$$\mathbf{B}' = \frac{\Gamma B_0}{E_0^2/c^2 + B^2} \left[ B_0 \mathbf{B} + \frac{E_0}{c^2} \mathbf{E} \right] \quad (11b)$$

They are therefore colinear because  $E_0 \mathbf{B}' = B_0 \mathbf{E}'$ . The frame velocity consequently simplifies into

$$\mathbf{V} = \frac{\mathbf{E} \wedge \mathbf{B}}{E_0^2/c^2 + B^2} \quad (12)$$

Note in this expression the mixing between field strengths in both frames, one with subscript 0 and the other without any subscript. There exists however a symmetry in the sense that  $E_0^2 + c^2 B^2 = E^2 + c^2 B_0^2$  so we can use either  $E_0$  or  $B_0$  but not both simultaneously. This velocity is always less than the speed of light if  $I_1 \neq 0$  and  $I_2 \neq 0$ . Therefore, there always exist a frame where  $\mathbf{E}$  and  $\mathbf{B}$  are parallel, whatever the strength of  $\mathbf{E}$  compared to  $\mathbf{B}$ . The vanishing magnetic  $\mathbf{B} = 0$  or electric  $\mathbf{E} = 0$  field are special cases of the general treatment presented here the second one reducing to the electric drift motion.

The special case of a null field for which  $I_1 = I_2 = 0$  is treated separately because then  $E = cB$  and the speed of the frame is exactly equal to  $c$  and thus is not a physical frame. It will be treated separately.

### 3.2. Motion in the frame where $\mathbf{E}$ and $\mathbf{B}$ are parallel

In the previous section, we showed that it is always possible to reduce the problem of particle motion into a configuration where  $\mathbf{E}$  and  $\mathbf{B}$  are parallel except for light like fields.. In this frame, integration of the trajectory is particularly simple when expressed in terms of the proper time  $\tau$  of the particle. Any electromagnetic field configuration can always be reduced to a parallel electric and magnetic field by an appropriate change of reference. In order not to overload the notations, in this and the following subsections we omit the primes to designate the quantities expressed in the frame  $K'$  where  $\mathbf{E}$  and  $\mathbf{B}$  are parallel. The integration of the equation of motion of a charged particle in such a field is relatively simple and straightforward. Indeed, let's consider an electromagnetic field such that  $\mathbf{E}$  and  $\mathbf{B}$  are directed along the  $e_z$  axis in a Cartesian coordinate system. The initial position of the particle is  $(x_0, y_0, z_0)$  and its initial velocity is  $\mathbf{v} = (v_x^0, v_y^0, v_z^0)$ . The equation of motion in covariant form is

$$\frac{dp^i}{d\tau} = q F^{ik} u_k \quad (13)$$

or in terms of the 4-velocity only

$$\frac{du^i}{d\tau} = \frac{q}{m} F^{ik} u_k \quad (14)$$

$u^i = (\gamma c, \gamma \mathbf{v})$  is the 4-velocity and  $p^i = m u^i$  the 4-momentum. In the Cartesian coordinate system, the electromagnetic field tensor is anti-diagonal and given by

$$F^{ik} = \begin{pmatrix} 0 & 0 & 0 & -E/c \\ 0 & 0 & -B & 0 \\ 0 & B & 0 & 0 \\ E/c & 0 & 0 & 0 \end{pmatrix}. \quad (15)$$

Introducing  $\omega_E = \frac{qE}{mc}$  and  $\omega_B = \frac{qB}{m}$ , the equation of motion reduces to

$$\frac{du^0}{d\tau} = \frac{q}{m} F^{03} u_3 = -\omega_E u_3 \quad (16a)$$

$$\frac{du^1}{d\tau} = \frac{q}{m} F^{12} u_2 = -\omega_B u_2 \quad (16b)$$

$$\frac{du^2}{d\tau} = \frac{q}{m} F^{21} u_1 = +\omega_B u_1 \quad (16c)$$

$$\frac{du^3}{d\tau} = \frac{q}{m} F^{30} u_0 = +\omega_E u_0 \quad (16d)$$

All the components of the 4-velocity are brought back to their contravariant expressions so that by index elevation  $u^i = \eta^{ik} u_k$ . This implies that  $u^0 = u_0$  for the temporal index and  $u^a = -u_a$  for the spatial indices. The system decouples into two size 2 subsystems each so that

$$\frac{du^0}{d\tau} = \omega_E u^3 \quad (17a)$$

$$\frac{du^1}{d\tau} = \omega_B u^2 \quad (17b)$$

$$\frac{du^2}{d\tau} = -\omega_B u^1 \quad (17c)$$

$$\frac{du^3}{d\tau} = \omega_E u^0. \quad (17d)$$

Two variables are eliminated to reduce the system to the velocity components  $u^0$  and  $u^1$  only

$$\frac{d^2 u^0}{d\tau^2} = \omega_E^2 u^0 \quad (18a)$$

$$\frac{d^2 u^1}{d\tau^2} = -\omega_B^2 u^1 \quad (18b)$$

The general solutions are given by

$$u^0 = A e^{\omega_E \tau} + B e^{-\omega_E \tau} \quad (19a)$$

$$u^1 = C \cos(\omega_B \tau) + D \sin(\omega_B \tau) \quad (19b)$$

At initial time, we have  $t = t_0$  corresponding to  $\tau = 0$  and  $\mathbf{v} = v_0 \mathbf{t}$  thus  $\mathbf{u}^0 = \gamma_0 (c, \mathbf{v}_0)$  with  $\gamma_0 = (1 - (\beta_0)^2)^{-1/2}$ . These initial conditions enforce

$$A = \gamma_0 \frac{c + v_0^z}{2} \quad (20a)$$

$$B = \gamma_0 \frac{c - v_0^z}{2} \quad (20b)$$

$$C = \gamma_0 v_0^x \quad (20c)$$

$$D = \gamma_0 v_0^y \quad (20d)$$

thus the 4-velocity evolution given in terms of the proper time according to

$$u^0 = \gamma_0 c \left[ \text{ch}(\omega_E \tau) + \beta_0^z \text{sh}(\omega_E \tau) \right] \quad (21a)$$

$$u^3 = \gamma_0 c \left[ \text{sh}(\omega_E \tau) + \beta_0^z \text{ch}(\omega_E \tau) \right] \quad (21b)$$

$$u^1 = \gamma_0 c \left[ \beta_0^x \cos(\omega_B \tau) + \beta_0^y \sin(\omega_B \tau) \right] \quad (21c)$$

$$u^2 = \gamma_0 c \left[ -\beta_0^x \sin(\omega_B \tau) + \beta_0^y \cos(\omega_B \tau) \right] \quad (21d)$$

All that remains is to integrate with respect to the proper time to find the trajectory of the particle

$$c(t - t_0) = \frac{\gamma_0 c}{\omega_E} \left[ \text{sh}(\omega_E \tau) + \beta_0^z (\text{ch}(\omega_E \tau) - 1) \right] \quad (22a)$$

$$x - x_0 = \frac{\gamma_0 c}{\omega_B} \left[ \beta_0^x \sin(\omega_B \tau) - \beta_0^y (\cos(\omega_B \tau) - 1) \right] \quad (22b)$$

$$y - y_0 = \frac{\gamma_0 c}{\omega_B} \left[ \beta_0^x (\cos(\omega_B \tau) - 1) + \beta_0^y \sin(\omega_B \tau) \right] \quad (22c)$$

$$z - z_0 = \frac{\gamma_0 c}{\omega_E} \left[ (\text{ch}(\omega_E \tau) - 1) + \beta_0^z \text{sh}(\omega_E \tau) \right] \quad (22d)$$

The trajectory of the particle is thus entirely determined as a function of proper time  $\tau$  in an analytical way with simple expressions including trigonometric and hyperbolic functions. These equations for 4-velocity and 4-position are implemented in the code.

Note that the equation of motion could be resolved immediately in the observer's frame of reference by diagonalizing the tensor of the electromagnetic field  $F^{ik}$ . This would be the same as the change of reference frame made above (Vandervoort, 1960).

For testing the numerical algorithm and the limiting Lorentz factor due to numerical round off error, we check the implementation on a purely electric and a purely magnetic field.

### 3.3. Vanishing magnetic field

In the case of a vanishing magnetic field  $\mathbf{B} = 0$ , the frame  $K$  and  $K'$  are identical and there is no need to boost from one frame to the other. The 4-velocity reduces to

$$u^0 = \gamma_0 c \left[ \text{ch}(\omega_E \tau) + \beta_0^z \text{sh}(\omega_E \tau) \right] \quad (23a)$$

$$u^1 = \gamma_0 c \beta_0^x \quad (23b)$$

$$u^2 = \gamma_0 c \beta_0^y \quad (23c)$$

$$u^3 = \gamma_0 c \left[ \text{sh}(\omega_E \tau) + \beta_0^z \text{ch}(\omega_E \tau) \right] \quad (23d)$$

and the trajectory simply into

$$c(t - t_0) = \frac{\gamma_0 c}{\omega_E} \left[ \text{sh}(\omega_E \tau) + \beta_0^z (\text{ch}(\omega_E \tau) - 1) \right] \quad (24a)$$

$$x - x_0 = \gamma_0 c \beta_0^x \tau \quad (24b)$$

$$y - y_0 = \gamma_0 c \beta_0^y \tau \quad (24c)$$

$$z - z_0 = \frac{\gamma_0 c}{\omega_E} \left[ (\text{ch}(\omega_E \tau) - 1) + \beta_0^z \text{sh}(\omega_E \tau) \right]. \quad (24d)$$

### 3.4. Vanishing electric field

In the case of a vanishing electric field  $\mathbf{E} = 0$ , the frame  $K$  and  $K'$  are again identical and there is no need to boost from one frame to the other. The 4-velocity reduces to

$$u^0 = \gamma_0 c \quad (25a)$$

$$u^1 = \gamma_0 c \left[ \beta_0^x \cos(\omega_B \tau) + \beta_0^y \sin(\omega_B \tau) \right] \quad (25b)$$

$$u^2 = \gamma_0 c \left[ -\beta_0^x \sin(\omega_B \tau) + \beta_0^y \cos(\omega_B \tau) \right] \quad (25c)$$

$$u^3 = \gamma_0 c \beta_0^z \quad (25d)$$



All that remains is to integrate with respect to the proper time to find the trajectory of the particle

$$(t - t_0) = \gamma_0 \tau \quad (26a)$$

$$x - x_0 = \frac{\gamma_0 c}{\omega_B} \left[ \beta_0^x \sin(\omega_B \tau) - \beta_0^y (\cos(\omega_B \tau) - 1) \right] \quad (26b)$$

$$y - y_0 = \frac{\gamma_0 c}{\omega_B} \left[ \beta_0^x (\cos(\omega_B \tau) - 1) + \beta_0^y \sin(\omega_B \tau) \right] \quad (26c)$$

$$z - z_0 = \gamma_0 c \beta_0^z \tau = v_0^z (t - t_0) \quad (26d)$$

Testing our algorithm in a constant and uniform electromagnetic field is meaningless because the solution is known analytically in any reference frame. Even the force-free field test introduced by Ripperda et al. (2017) and not tested in Ptri (2017) is included in this analytical exact solution as demonstrated in the next paragraph. However, for numerical purposes, it is desirable to check the ability of our code to handle very high Lorentz factor above  $\gamma = 10^{12}$  to look for round-off errors and possible issues related to finite digit precision.

### 3.5. Motion in the frame where $\mathbf{E}$ and $\mathbf{B}$ are perpendicular

When electric and magnetic fields are perpendicular, the second invariant vanishes  $\mathcal{I}_2 = 0$ , there exist always a frame where either the electric or the magnetic field vanishes depending on the sign of the invariant  $\mathcal{I}_1$ . We are then back to the previous cases for a pure electric or magnetic field. Indeed, if  $\mathcal{I}_1 > 0$  the constant  $\alpha = c^2/E^2$  and therefore the velocity of the frame where  $\mathbf{B}$  vanishes is

$$\mathbf{V}_B = \frac{\mathbf{E} \wedge \mathbf{B}}{E^2} c^2. \quad (27)$$

If  $\mathcal{I}_1 < 0$  the constant  $\alpha = 1/B^2$  and therefore the velocity of the frame where  $\mathbf{E}$  vanishes is

$$\mathbf{V}_E = \frac{\mathbf{E} \wedge \mathbf{B}}{B^2} \quad (28)$$

that is the usual electric drift frame. Consequently, the cases  $\mathcal{I}_1 \neq 0$  and  $\mathcal{I}_2 = 0$  are included in the previous sections.

### 3.6. Light like electromagnetic field

Nevertheless, the case where both electromagnetic invariants vanish  $\mathcal{I}_1 = \mathcal{I}_2 = 0$  must be treated separately because there exists no physical frame moving at a speed strictly less than  $c$  where either  $\mathbf{E}$  or  $\mathbf{B}$  vanishes. Going back to the equation of motion let us assume that the electric field is along  $\mathbf{E} = E \mathbf{e}_y$  and the magnetic field along  $\mathbf{B} = B \mathbf{e}_z$ . The electromagnetic tensor then reduces to

$$F^{ik} = \begin{pmatrix} 0 & 0 & -E/c & 0 \\ 0 & 0 & -B & 0 \\ E/c & B & 0 & 0 \\ 0 & 0 & 0 & 0 \end{pmatrix} \quad (29)$$

The equation of motion therefore becomes

$$\frac{du^0}{d\tau} = \omega_E u^2 \quad (30a)$$

$$\frac{du^1}{d\tau} = \omega_B u^2 \quad (30b)$$

$$\frac{du^2}{d\tau} = (\omega_E u^0 - \omega_B u^1) \quad (30c)$$

$$\frac{du^3}{d\tau} = 0. \quad (30d)$$

The last equation integrates into  $u^3 = u_0^3 = \text{constant}$  and the trajectory is constraint to follow  $z - z_0 = u_0^3 (\tau - \tau_0)$ . Eliminating  $u^0$  and  $u^1$  from the equation evolving  $u^2$  we find

$$\frac{d^2 u^2}{d\tau^2} + (\omega_B^2 - \omega_E^2) u^2 = 0. \quad (31)$$

Three cases must be distinguished

1. a dominant electric field for  $\omega_E > \omega_B$ .
2. a dominant magnetic field for  $\omega_B > \omega_E$ .
3. a light like field if  $\omega_E = \omega_B$ .

Note that  $\omega_E^2 - \omega_B^2$  is related to the relativistic invariant  $I_1$  through  $\frac{q^2}{m^2 c^3} I_1 = \omega_E^2 - \omega_B^2$ .

In an light like electromagnetic field, there is no frame where  $\mathbf{E}$  or  $\mathbf{B}$  vanishes. A plane electromagnetic wave propagating in vacuum is a typical example. In this field, the two Lorentz invariants vanish  $I_1 = I_2 = 0$ . The equation for the 4-velocity reduces to

$$\frac{d^2 u^2}{d\tau^2} = 0 \quad (32)$$

whose solution is  $u^2 = C \tau + \gamma_0 v_0^y$  where  $C$  is a constant of integration. The other two components are

$$u^0 = \omega_E \left( C \frac{\tau^2}{2} + \gamma_0 v_0^y \tau \right) + \gamma_0 c \quad (33a)$$

$$u^1 = \omega_B \left( C \frac{\tau^2}{2} + \gamma_0 v_0^y \tau \right) + \gamma_0 v_0^x. \quad (33b)$$

Replacing in  $du^2/d\tau$  we find  $C = \gamma_0 \omega_B c (1 - \beta_0^x)$  because  $\omega_E = \omega_B$ . The solution is therefore

$$u^0 = \gamma_0 c \left[ 1 + (1 - \beta_0^x) \frac{(\omega_B \tau)^2}{2} + \beta_0^y \omega_B \tau \right] \quad (34a)$$

$$u^1 = \gamma_0 c \left[ \beta_0^x + (1 - \beta_0^x) \frac{(\omega_B \tau)^2}{2} + \beta_0^y \omega_B \tau \right] \quad (34b)$$

$$u^2 = \gamma_0 c \left[ \beta_0^y + (1 - \beta_0^x) \omega_B \tau \right] \quad (34c)$$

$$u^3 = \gamma_0 v_0^z. \quad (34d)$$

Performing another integration gives the explicit form of the trajectory as

$$c(t - t_0) = \gamma_0 c \left[ \tau + (1 - \beta_0^x) \frac{\omega_B^2 \tau^3}{6} + \beta_0^y \frac{\omega_B \tau^2}{2} \right] \quad (35a)$$

$$x - x_0 = \gamma_0 c \left[ \beta_0^x \tau + (1 - \beta_0^x) \frac{\omega_B^2 \tau^3}{6} + \beta_0^y \frac{\omega_B \tau^2}{2} \right] \quad (35b)$$

$$y - y_0 = \gamma_0 c \left[ \beta_0^y \tau + (1 - \beta_0^x) \frac{\omega_B \tau^2}{2} \right] \quad (35c)$$

$$z - z_0 = \gamma_0 v_0^z \tau. \quad (35d)$$

These solutions must be included in the algorithm whenever both invariants vanish. Tests will be performed in a linearly and a circularly polarized plane electromagnetic wave in section 5.

### 3.7. Force-free field

In the special case of a force-free field, the electric and magnetic field are perpendicular according to the expression

$$\mathbf{E} + \mathbf{V} \wedge \mathbf{B} = \mathbf{0} \quad (36)$$

where  $\mathbf{V}$  is the particle velocity in the frame  $K$ . In that case, by construction  $\mathbf{E} \cdot \mathbf{B} = 0$  and  $E < cB$ . The privileged frame  $K'$  according to the general transformation rule is therefore simply the electric drift frame moving at a velocity

$$\mathbf{V}_E = \frac{\mathbf{E} \wedge \mathbf{B}}{B^2} = \mathbf{V} = \mathbf{V}_{\parallel}. \quad (37)$$

Consequently the particle velocity  $\mathbf{V}$  is equal to the drift velocity  $\mathbf{V}_E$  and equal to  $\mathbf{V}_{\parallel}$  meaning that in the frame where  $\mathbf{E}$  and  $\mathbf{B}$  are parallel (actually  $\mathbf{E} = 0$ ) the particle is at rest. Thus no Lorentz force acts at all in  $K'$  because initially  $\mathbf{V}' = 0$  and  $\mathbf{E}' = 0$ , the particle remains at rest forever in  $K'$  as long as the force-free condition eq. (36) is satisfied, whatever the value of  $\mathbf{B}'$ . This result is analytically exact, there is no numerical error, even to round off accuracy, contrasting severely with other algorithms showing a slowly breaking of the force-free motion (Ripperda et al., 2017).

### 3.8. Low electric and magnetic field

The expression for particle trajectories given in eq. (22) cannot be applied straightforwardly whenever  $\omega_E$  or  $\omega_B$  tends to zero because they appear in the denominator of some expressions. However, to include these cases in the general algorithm we designed, we performed a first order expansion whenever required to smoothly join the vanishing electric or magnetic field case presented previously.

In regions where the electric field is weak according to the condition  $\omega_E \tau \ll 1$  the time and  $z$  components are integrated according to

$$(t - t_0) = \gamma_0 \tau \quad (38a)$$

$$z - z_0 = v_0^z (t - t_0). \quad (38b)$$

In regions where the magnetic field is weak according to the condition  $\omega_B \tau \ll 1$  the  $x$  and  $y$  components are integrated according to

$$x - x_0 = \gamma_0 c \beta_0^x \tau \quad (38c)$$

$$y - y_0 = \gamma_0 c \beta_0^y \tau. \quad (38d)$$

Taking into account these two limiting cases of vanishing electric or magnetic field, our algorithm can handle with any field strength and any geometry of the electromagnetic field as long as these fields are constant in time and uniform in space. Thus its robustness must be tested against spatially and temporally varying fields. This is checked in the next section. Nevertheless, our focus in this paper is about ultra-relativistic regime of particle motion, dealing with Lorentz factor as high as  $\gamma = 10^{12}$ . Although the analytical expressions are obviously valid for any  $\gamma$ , the finite precision of numerical implementation of any algorithm limits the possible range of Lorentz factor achievable. Therefore, we will also check our code on simple test cases such as purely electric or purely magnetic field in order to assess the stringent limitations of what can be done numerically with ultra-relativistic plasmas.

But before running simulations, we have to properly choose the optimal time step to evolve the particle motion. This crucial problem is addressed in the following section.

## 4. Simulation time step determination

In the previous section, we showed that the equation of motion is most easily solved by introducing the particle proper time and 4-velocity. Its time evolution could be performed by imposing and advancing the proper time. However, this is not the way numerical simulations are performed. We need to fix the observer time step  $\Delta t$  in the frame  $K$  and not the proper time step  $\Delta \tau$  in the particle rest frame. In this section, we show that the proposed numerical scheme can be used in Particle-In-Cell simulations that is with a fixed observer time step  $\Delta t$ . A PIC code uses discrete time steps in terms of the time in the frame of the simulation. The proposed scheme, on the other hand, uses discrete time steps in terms of the proper time  $\Delta \tau$  of each particle. Now, for a given time step in the frame of the simulation  $\Delta t$ , we retrieve the corresponding time step in terms of proper time  $\Delta \tau$  for each particle. This requires to solve a non-linear equation. To make the scheme applicable to PIC simulations, we include a detailed discussion on this issue, deriving the equation to solve when calculating the time step in terms of proper time for each particle and how to solve it.

### 4.1. Time step setting in different frames

In a first step, the relation between particle proper time  $\Delta \tau$  and the time  $\Delta t'$  in frame  $K'$ , eq. (22) can be inverted analytically to give

$$\omega_E \Delta \tau = \log \left( \frac{\xi + \sqrt{1 - (\beta_0^z)^2 + \xi^2}}{1 + \beta_0^z} \right) \quad (39)$$

where we introduced  $\xi = \omega_E \Delta t' / \gamma_0 + \beta_0^z$ . This expression is optimal for numerical computation, working also when  $\beta_0^z$  is nearly one. In a second step, the time  $\Delta t'$  must be related to the observer time  $\Delta t$  in frame  $K$ , the one used in the simulation to advance time one time step.  $\Delta t$  and  $\Delta t'$  are related by a Lorentz boost similar to eq. (4) written most efficiently as

$$\Delta t = \Gamma \left( \Delta t' - \frac{\mathbf{V} \cdot \Delta \mathbf{r}'}{c^2} \right) \quad (40)$$

where  $\Gamma = (1 - V^2/c^2)^{-1/2}$ . The particle advance in position  $\Delta \mathbf{r}'$  in frame  $K'$  is known analytically from eq. (22) if  $\Delta \tau$  is known. Symbolically, we write  $\Delta \mathbf{r}'(\Delta \tau)$ . Moreover,  $\Delta \tau$  is found from  $\Delta t'$  thanks to eq. (39) or symbolically  $\Delta \tau(\Delta t')$  thus  $\Delta t$  is found from solving the non-linear scalar equation 40, remembering that finally  $\Delta \mathbf{r}'(\Delta t)$ .

This procedure is best understood by a simple example. Let us consider a particle moving along an arbitrary direction in frame  $K$  with constant speed  $\mathbf{v}$ . In the frame  $K'$ , it moves at a constant speed  $\mathbf{v}'$ ,  $K'$  moving with respect to  $K$  at a speed  $\mathbf{V}$ . How to relate then the speeds  $\mathbf{v}$  and  $\mathbf{v}'$  knowing the trajectory in  $K'$ ?

In this simple case, the vector position is given in frame  $K'$  by  $\Delta \mathbf{r}' = \mathbf{v}' \Delta t'$ . Therefore  $\Delta t'$  can be solved with respect to  $\Delta t'$  as

$$\Delta t' = \frac{\Delta t}{\Gamma(1 + \mathbf{V} \cdot \mathbf{v}'/c^2)} \quad (41)$$

$\Delta \mathbf{r}$  is then related to  $\Delta \mathbf{r}'$  via the spatial part of the Lorentz transformation. In such a way, the velocity

$$\mathbf{v} = \frac{\Delta \mathbf{r}}{\Delta t} = \frac{\mathbf{v}'}{\Gamma(1 + \mathbf{V} \cdot \mathbf{v}'/c^2)} + \left(1 + \frac{\Gamma}{\Gamma + 1} (\mathbf{V} \cdot \mathbf{v}'/c^2)\right) \frac{\mathbf{V}}{1 + \mathbf{V} \cdot \mathbf{v}'/c^2} \quad (42)$$

is computed from the velocity in the frame  $K'$ . It can be checked that the results agree with the relativistic composition of velocities. The crucial point in this derivation is the analytical inversion of the relation  $\Delta t(\Delta t')$  into  $\Delta t'(\Delta t)$ . This is no more the case for a particle in an electromagnetic. We therefore have to resort to numerical inversion by some root finding methods like Newton-Raphson scheme or other techniques as described for instance in Press (2007).

#### 4.2. Adaptive time steps

The optimal time step strongly depends on the local value of the electromagnetic field and on the particle velocity. Due to the Lorentz transformation of the electromagnetic tensor and because of time dilation, for ultra-relativistic particles, we expect a significant gain in time computation when this time step is adaptively adjusted to the local fields and particle velocities. In order to improve and better control the accuracy of our numerical solution from time step to time step, we implemented also a semi-implicit iterative scheme where the actual constant electromagnetic field employed to advance the particle is the one located midway between the time and position of the particle at the instant  $t^n$  and  $t^{n+1}$ . It resembles the algorithm we already used in Ptri (2017). If the solution does not converge to a prescribed precision after a limited number of iteration  $N_{\max}$  (we set it to  $N_{\max} = 10$ ), the time step is decreased by a factor 2 and the process starts again with at most  $N_{\max}$  iterations. If necessary the time step is again diminished by a factor 2 until convergence is reached. Table 2 summarized the pseudo-code used to advance the particle position one time step by using the adaptive scheme.

Having one an algorithm to impose a fixed or prescribed *observer time step*, we can coupling the particle orbit integrator to the field advance like any other existing PIC code. There is not special care to first advance particles and second to compute the new fields. Let us now look at some particular tests of our algorithm.

### 5. Numerical tests in spatially and temporally varying fields

We extensively tested our new algorithm first against trivial configurations of an uniform electric or magnetic field, then in a cross electric and magnetic field following the electric drift frame. More stringent tests like the electrostatic Kepler problem, the magnetic gradient drift and motion in an ultra-strong linearly or circularly polarized plane wave are also considered.

#### 5.1. Normalisations and adimensionalisations

Before showing some numerical results, we normalize the relevant quantities to characteristic values. As we deal with relativistic motion, the speed is conveniently normalized to the speed of light  $c$ . Next we introduce a characteristic frequency  $\omega$  related the electromagnetic frequencies  $\omega_B$  or  $\omega_E$  depending on the problem studied. This naturally leads to a characteristic length given by  $c/\omega$ . Moreover, a normalized time is then introduced by  $\tilde{t} = \omega t$ . In the simulation results shown below, we will always refer to these normalised quantities and plot graphs according to this convention. Concretely, for simulation purposes, we specify the charge  $q$  and mass  $m$  of the particle in the different tests such that  $q = 1$  and  $m = 1$ .

---

**Algorithm 2:** The algorithm to advance the particle position one time step with a prescribed accuracy  $\epsilon$ .

---

**Input:** The initial 4-position and 4-velocity of the particle  $(\mathbf{x}^n, \mathbf{u}^n)$  at time  $t^n$ .

**Output:** The final 4-position and 4-velocity of the particle  $(\mathbf{x}^{n+1}, \mathbf{u}^{n+1})$  at time  $t^{n+1}$ .

```

/* First guess position and velocity */
1 Compute the first guess  $(\mathbf{x}^{n+1}, \mathbf{u}^{n+1})$  from  $\mathbf{E}^n$  and  $\mathbf{B}^n$ .
2 Compute the first guess fields  $\mathbf{E}^{n+1}$  and  $\mathbf{B}^{n+1}$  at  $\mathbf{x}^{n+1}$ .
/* Number of iterations to converge */
3 it=0
/* The iteration loop until convergence to accuracy  $\epsilon$  */
4 do
5     it++;
6     Compute the midway fields  $\mathbf{E}^*$  and  $\mathbf{B}^*$  from the midway position  $\mathbf{x}^* = (\mathbf{x}^n + \mathbf{x}^{n+1})/2$ ;
7     Integrate trajectory to guess new  $(\mathbf{x}^{n+1}, \mathbf{u}^{n+1})$  from  $\mathbf{E}^*$  and  $\mathbf{B}^*$ ;
8     Find the new fields  $\mathbf{E}_g^{n+1}$  and  $\mathbf{B}_g^{n+1}$  at  $\mathbf{x}^{n+1}$ ;
9     Compute the difference  $\Delta\mathbf{E} = \mathbf{E}_g^{n+1} - \mathbf{E}^{n+1}$  and  $\Delta\mathbf{B} = \mathbf{B}_g^{n+1} - \mathbf{B}^{n+1}$ ;
10    Update by setting  $\mathbf{E}_g^{n+1} = \mathbf{E}^{n+1}$  and  $\mathbf{B}_g^{n+1} = \mathbf{B}^{n+1}$ ;
/* If more iterations than  $N_{\max}$  required */
11    if ( $it > N_{\max}$ ) then
12         $\Delta t = \Delta t/2$ ; // reduce time step by 2
13        it = 0; // Start a new cycle of iterations
14 while ( $(\Delta\mathbf{E}, \Delta\mathbf{B}) > \epsilon$ ) // looking for accuracy  $\epsilon$ 
15

```

---

**Table 2.** Pseudo-code summarizing the Picard iteration scheme.

## 5.2. Purely electric field

Let us start with a homogeneous and uniform electric field. Take as an initial condition  $t_0 = 0$  and the position of the particle to be  $x_0 = y_0 = z_0 = 0$  with no initial velocity such that  $\boldsymbol{\beta} = \mathbf{0}$  and thus  $\gamma_0 = 1$ . The particle world line is therefore a straight line parametrized with respect to its proper time  $\tau$  according to

$$\omega_E t = \text{sh}(\omega_E \tau) \quad (43a)$$

$$x = 0 \quad (43b)$$

$$y = 0 \quad (43c)$$

$$\omega_E z = c [\text{ch}(\omega_E \tau) - 1]. \quad (43d)$$

Expressed in terms of the observer time  $t$ , the trajectory and velocity become

$$\omega_E z = c \left[ \sqrt{1 + (\omega_E t)^2} - 1 \right] \quad (44a)$$

$$\frac{v_z}{c} = \frac{\omega_E t}{\sqrt{1 + (\omega_E t)^2}}. \quad (44b)$$

The Lorentz factor grows in time  $t$  according to

$$\gamma = \text{ch}(\omega_E \tau) = \sqrt{1 + (\omega_E t)^2}. \quad (45)$$

Note that the only relevant time scale in this problem is the normalized quantity  $\tilde{t} = \omega_E t$  or  $\tilde{\tau} = \omega_E \tau$ .

An example of accelerating electric field is shown in fig. 1 for the position in blue and for the Lorentz factor in red. What matters is not the particle charge and mass, but the quantity  $qE/mc = \omega_E$  which gives the typical time scale for acceleration. The time step in the observer frame  $\Delta t$  is imposed by the user. We took an initial value of  $\omega_E \Delta t = 10^{-6}$  although there is no restriction on  $\Delta t$ . Indeed, after each iteration we multiplied it by 2 in order to show the flexibility of adapting the *observer time step*. Then the proper time step  $\Delta \tau$  is computed according to eq. (39). The particle first

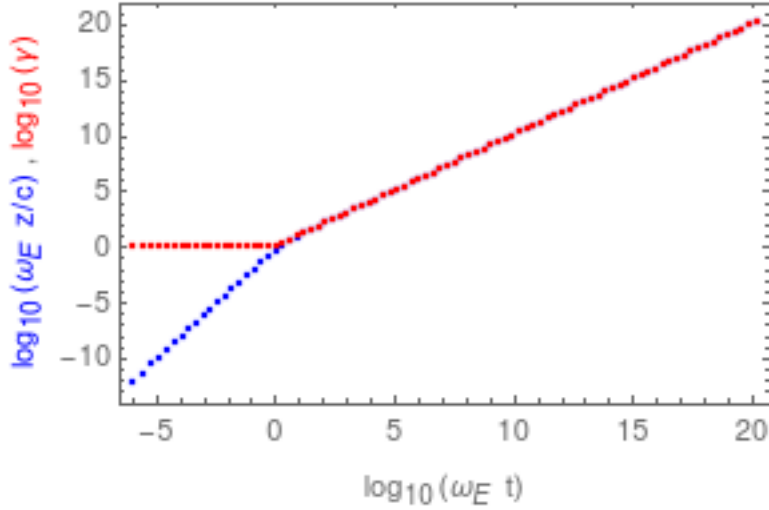


Fig. 1. Position in blue and Lorentz factor in red of an electron in the accelerating electric field  $E_z$  and with constant observer time step  $\Delta t$ .

accelerates in the Newtonian regime with a quadratic increase in position  $z$  up to the point where it reaches almost the speed of light. After a time  $\omega_E t \gtrsim 1$  it goes at almost constant speed  $v_z \approx c$ . The Lorentz factor then increases almost linearly with time  $\gamma \approx \omega_E t$ . We let the particle gain energy up to  $\gamma = 10^{20}$  to check possible issues related to numerical round off and truncation. No special problems were met for these ultra-relativistic speeds.

### 5.3. Purely magnetic field

Let us go on with a homogeneous and uniform magnetic field. Take as an initial condition  $t_0 = 0$  and the position of the particle in the  $xOy$  plane such that  $x_0 = z_0 = 0$  and  $y_0 = \gamma_0 v_0^x / \omega_B = r_L$  with initial velocity such that  $\boldsymbol{\beta} = (\beta_0^x, 0, \beta_0^z)$ .  $r_L = \gamma v / \omega_B$  is the Larmor radius of the trajectory. The Lorentz factor is constant and given by  $\gamma = \gamma_0$ . The particle world line is therefore

$$t = \gamma_0 \tau \quad (46a)$$

$$x = r_L \sin(\omega_B \tau) \quad (46b)$$

$$y = r_L \cos(\omega_B \tau) \quad (46c)$$

$$z = v_0^z t. \quad (46d)$$

The particle gyro-frequency is  $\omega_B$  in proper time but reduced to  $\omega_B / \gamma_0$  in the observer frame as is well known from special relativity. In the observer frame, the relevant normalized time scale is therefore  $\omega_B t$ . For an ultra-relativistic particle with  $v_0^x \approx c$ , its Larmor radius is  $r_L \approx \gamma_0 c / \omega_B$ , the expression used in the introduction. An example is shown in Fig. 2 for  $B = 1$  and  $\gamma = 10^{10}$ . The time step is set to  $\omega_B \Delta\tau = 10^{-2}$ . The radius of the orbit stay at  $r_L$  to very high accuracy, more than 15 digits of precision. The Lorentz factor remains constant and equal to  $\gamma_0$  as expected.

### 5.4. Cross electric and magnetic fields

As another proof of the efficiency of the algorithm, we compute the trajectories in a crossed electromagnetic field ( $\mathbf{E} \cdot \mathbf{B} = 0$ ) where the average motion is an electric drift in the  $\mathbf{E} \wedge \mathbf{B}$  direction at the electric drift speed  $\mathbf{v}_E = \mathbf{E} \wedge \mathbf{B} / B^2$ . In the frame moving at  $\mathbf{v}_E$  the electric field vanishes and the particle simply follows an helicoidal motion along the constant magnetic field, see the case treated in the previous paragraph. This motion is only allowed for weak electric fields satisfying  $E < c B$  thus enforcing  $v_E < c$ . For concreteness, let us assume an electric field directed along  $\mathbf{e}_y$  and a magnetic field directed along  $\mathbf{e}_z$ . The electric drift speed becomes  $\mathbf{v}_E = (E_y / B_z) \mathbf{e}_x$ . A Lorentz transformation of the electromagnetic field with Lorentz factor  $\Gamma_E = 1 / \sqrt{1 - v_E^2 / c^2}$  along  $\mathbf{v}_E$  shows that in the comoving frame

$$\mathbf{E}' = 0 \quad (47a)$$

$$\mathbf{B}' = \mathbf{B} / \Gamma_E. \quad (47b)$$

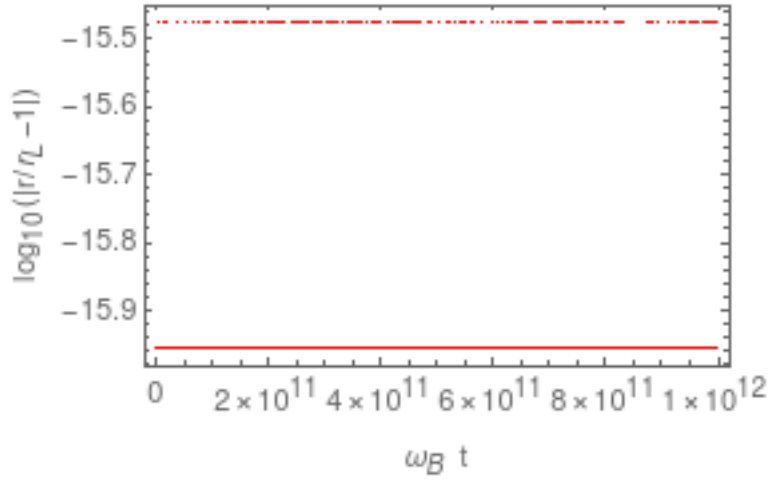


**Fig. 2.** Evolution of the error in the orbital radius of an electron in the uniform magnetic field with  $\gamma = 10^{10}$ .

The electric field vanishes as expected and the magnetic field is decreased potentially by a large ratio equal to the Lorentz factor of the comoving frame. As initial conditions for the particle position and velocity, we choose a helicoidal motion as explained in the previous paragraph and corresponding to an evolution in the solely magnetic field  $\mathbf{B}'$  as seen in the electric drift frame. These quantities are then transformed to the observer inertial frame according to Lorentz transformations for the three velocity  $\mathbf{v}$  of the particle. The algorithm is checked by computing the particle trajectory in the drift frame and the corresponding Lorentz factor of the particle that should remain constant in that frame. Using the Lorentz transformation the coordinates in the drift frame are

$$x' = \Gamma_E (x - v_E t) \quad (48a)$$

$$y' = y \quad (48b)$$

$$z' = z. \quad (48c)$$

For numerical purposes, the intensity of the electric field is set such that  $\Gamma_E = 10^3$ , the particle Lorentz factor in this drift frame is  $\gamma = 10^{10}$  and that of the magnetic field is  $B = 1$ . Typical results are depicted in fig. 3 for the trajectory in the electric drift frame which is usually an helicoidal motion and here exactly a circle in the comoving plane  $x'O'y'$ . The trajectory projected onto the  $x'O'y'$  plane remains a circle to very good accuracy with no change in radius within 8 digits, see Fig. 4. The accuracy seems less good than in the previous case for a purely magnetic field. We lost several digits in the computation of the Larmor radius. This loss of precision is imputed to the procedure used to evaluate the trajectory in the drift frame. Indeed, a Lorentz transform is required for the particle position as explained in eq.(48). This coordinate transform induced an additional error to the Larmor radius estimate. We lose several digits during the subtraction for  $x'$ . We checked that the error does not decrease with decreasing time step.

The most general and realistic fields are spatially and temporally varying. In these cases, the electromagnetic field has to be determined at some position and time during the particle motion. As severe tests of our algorithm, we study four problems of which three have exact analytical relativistic solutions for the particle trajectory. The relativistic electrostatic Kepler two body problem of an electron orbiting around a fixed positive ion is an interesting test for a spatially varying electric field. It is a central force case. The other two solutions correspond to a particle moving in a plane electromagnetic wave linearly or circularly polarized, a light like electromagnetic field. A last less trivial example is depicted by a particle drifting in the equatorial plane of a static magnetic dipole. We discuss in depth these regimes in the following paragraphs. The analytical solutions are described in Uzan and Deruelle (2014) and Gourgoulhon (2010). For completeness we recall them in the following paragraphs.

### 5.5. Central electric force

The two body problem in gravitational physics can be transposed in an equivalent electrostatic problem including relativistic velocity. In this case, a particle with charge  $q$  and mass  $m$  orbits around a fixed central particle with charge  $Q$ . For bounded orbits we require  $qQ < 0$ . Solutions are given by conservation of energy  $E$  (not to be

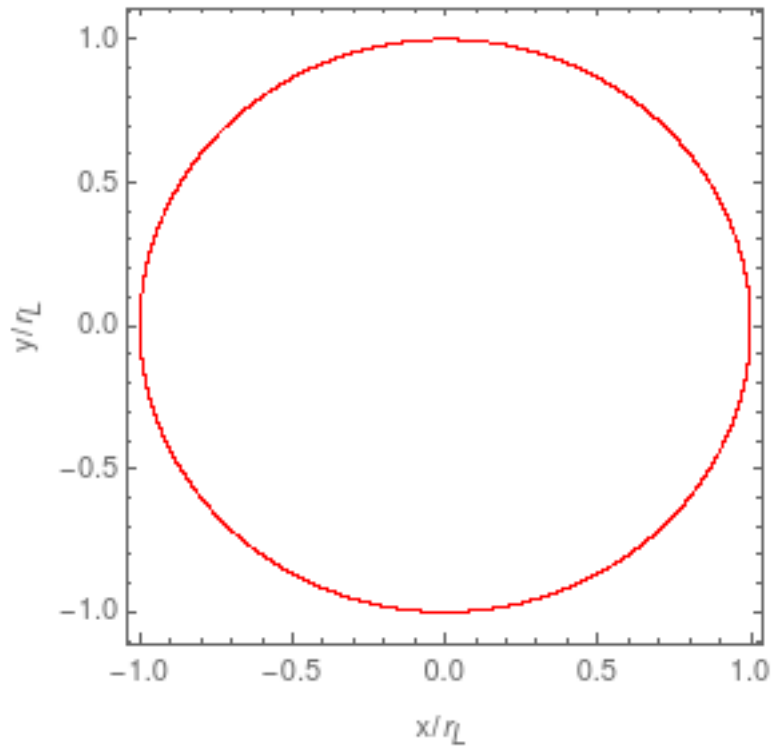


Fig. 3. Gyromotion of an electron in the electric drift frame with  $\Gamma_E = 10^3$  and  $\gamma = 10^{10}$ . The Larmor radius is  $r_L = 10^{10}$ .

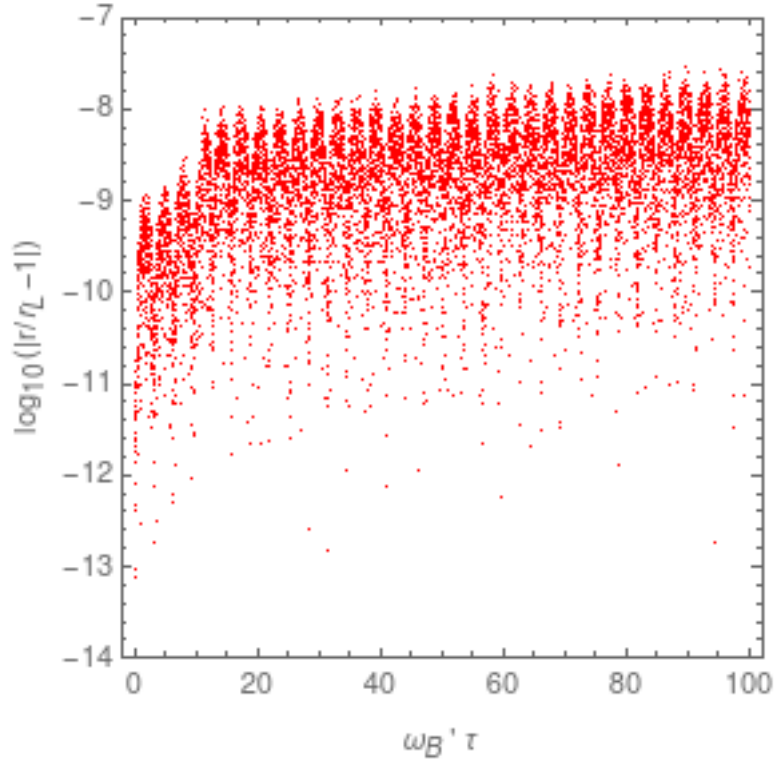


Fig. 4. Relative error in the Larmor radius computed from the transformation in eq.(48). The proper time  $\tau$  is shown on the  $x$  normalized to the cyclotron frequency in the electric drift frame.



confused with the electric field strength in this particular example) and angular momentum  $L$ . The electric force applied to the orbiting particle is

$$\mathbf{f} = \frac{qQ}{4\pi\epsilon_0 r^3} \mathbf{r}. \quad (49)$$

The orbital motion stays in a plane that we choose as the  $xOy$  plane. For  $\left| \frac{qQ}{4\pi\epsilon_0 Lc} \right| < 1$ , the general solution is

$$r(t) = \frac{p}{1 + e \cos(\Omega_p (\varphi(t) - \omega))} \quad (50a)$$

$$\Omega_p = \sqrt{1 - \left( \frac{qQ}{4\pi\epsilon_0 Lc} \right)^2} \quad (50b)$$

$$p = \frac{\Omega_p^2}{-\frac{qQ}{4\pi\epsilon_0 c^2} \frac{E}{L^2}} \quad (50c)$$

$$e^2 = \frac{1}{E^2} \left[ m^2 c^4 + \frac{E^2 - m^2 c^4}{\left( \frac{qQ}{4\pi\epsilon_0 Lc} \right)^2} \right]. \quad (50d)$$

The particle trajectory is plane and therefore described in a cylindrical coordinate system  $(r, \varphi)$  by the parametric function  $r(\varphi)$ . It depends implicitly on time  $t$  because of  $\varphi$  being a function of time  $t$  (the solution for  $\phi$  is not shown here). Note also that  $\Omega_p < 1$  meaning that the path is not a closed curved but a prograde precessing ellipse.  $p$  is called the orbital parameter and is related to the semi-major axis  $a$  and eccentricity of the ellipse via  $p = a(1 - e^2)$ . The periastron is located at a phase  $\omega$  with respect to the  $x$ -axis. These notations are common when studying stellar orbits in binary systems. This initial phase  $\omega$  is deduced from the initial condition  $r = r_0$  at  $\varphi = \varphi_0$ . Explicitly, we find

$$\Omega_p (\varphi_0 - \omega) = \arccos\left(\frac{p/r_0 - 1}{e}\right). \quad (51)$$

An example of relativistic particle trajectory showing the precession of the orbit is given in fig. 5. A piece of the exact analytical solution is also shown and matches perfectly the output of the numerical simulations. The total energy  $E$  is split into relativistic kinetic energy  $\gamma m c^2$  and electrostatic potential energy  $U$ . Inspection of fig. 6 demonstrates that the total energy is accurately conserved during time evolution. Angular momentum is also conserved to high accuracy, at least 6 digits, see the relative error evolving in time in fig.7. Finally, the relative error in the total energy  $\Delta E/E$  depending on time step is shown in fig. 8. We conclude that the scheme is second order in time, decreasing the error according to  $\Delta E/E \propto \Delta t^{-2}$ .

### 5.6. Magnetic drift in a dipole

The magnetic field created by a dipole of magnetic dipole moment  $\mu$  is given by the expression

$$\mathbf{B} = \frac{\mu_0}{4\pi r^3} \left( \frac{3(\mu \cdot \mathbf{r}) \mathbf{r}}{r^2} - \mu \right) \quad (52)$$

where  $\mu_0$  is the magnetic permeability. For a magnetic moment aligned with the  $z$ -axis, the magnetic field in the equatorial plane  $xOz$  is purely vertical and given by

$$B_z = B \frac{R^3}{r^3} \quad (53)$$

where  $B$  is the field strength at a distance  $R$  from the origin.

For non-relativistic particles, the magnetic gradient drift velocity depending on the perpendicular velocity  $v_\perp$  is given by (Baumjohann and Treumann, 1996)

$$\mathbf{v}_{\nabla B} = \frac{m v_\perp^2}{2qB} \frac{\mathbf{B} \wedge \nabla B}{B^2} \quad (54)$$

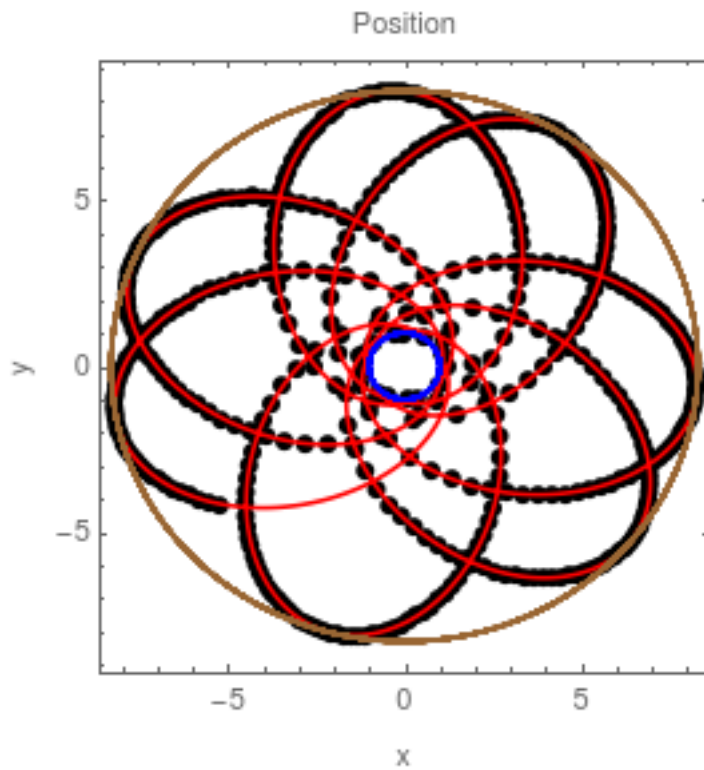


Fig. 5. Motion of an electron in the electric field of a fixed proton, black points. The relativistic precession of the orbit is clearly visible. The minimal and maximum radius of the orbit as predicted by the analytical formulae are shown by two circles tangent to the trajectory. A piece of the exact analytical solution is also shown in red.

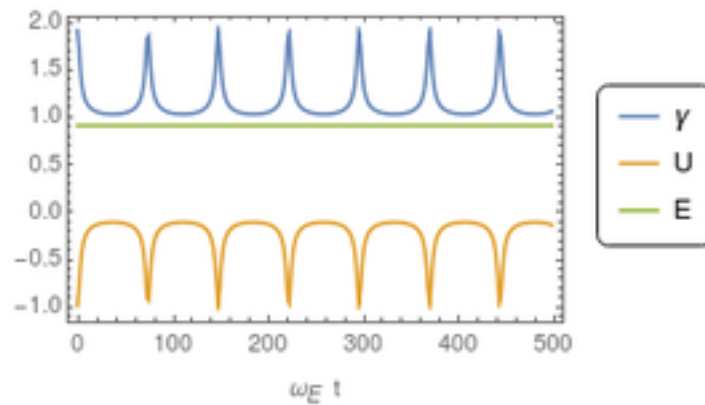


Fig. 6. Total energy  $E$ , relativistic kinetic energy  $\gamma m c^2$  and electrostatic potential energy  $U$  of an electron in the electric field of a fixed proton.  $E$  is accurately conserved, being a constant of motion.

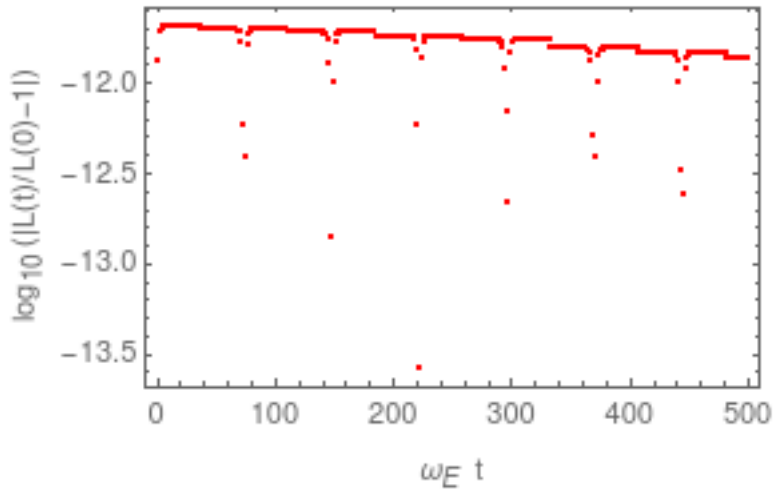


Fig. 7. Relative error in the angular momentum  $L$ .  $L$  is conserved within 11 digits.

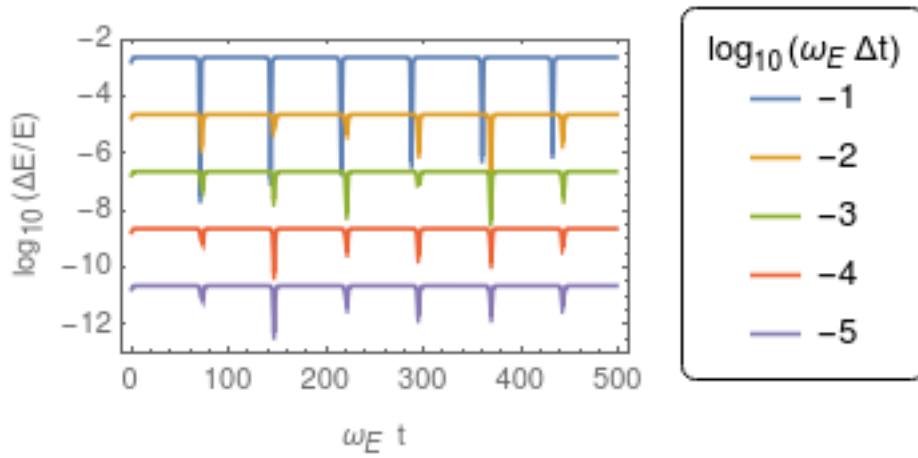


Fig. 8. Relative error in the total energy depending on time steps  $\Delta t$ .

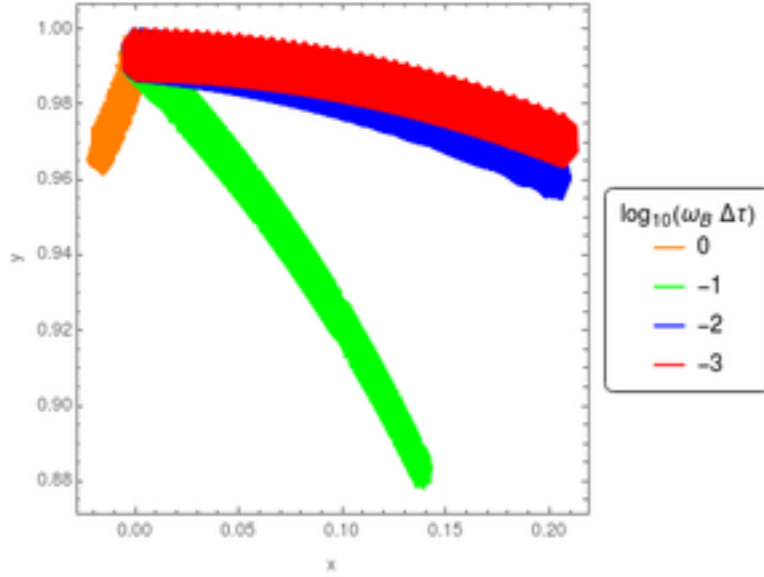


Fig. 9. Orbit of an electron in the equatorial plane of a magnetic dipole for  $B = 10^3$  and  $\gamma \approx 71$ .

For the above magnetic dipole geometry, in the equatorial plane we find a magnetic gradient velocity of

$$\mathbf{v}_{\nabla B} = \mp \frac{3}{2} \frac{m v_{\perp}^2}{q B r} \mathbf{e}_{\varphi} = \mp \frac{3}{2} \frac{v_{\perp}^2}{\omega_B r} \mathbf{e}_{\varphi} = \mp \frac{3}{2} v_{\perp} \frac{r_L}{r} \mathbf{e}_{\varphi} \quad (55)$$

solely directed into the azimuthal direction and decrease with distance as  $1/r$ .

Magnetic gradient drift motion is important in fields significantly varying on a length scale comparable to the Larmor radius. We study such motion in the equatorial plane of a magnetic dipole. We know that the particle must gyrate around the origin where the dipole is located. This motion is induced by the magnetic gradient drift in the azimuthal direction. The particle stay within two circles. An example of this drift motion is shown in fig. 9 for  $B = 10^3$  and  $\gamma \approx 71$ . The time step is varied and taken such that  $\log_{10}(\omega_B \Delta\tau) = \{0, -1, -2, -3\}$ . The Lorentz factor is conserved as is easily checked. The observed drift speed is compared to the expected drift speed in fig. 10. For a gyromotion well resolved in the proper time ( $\omega_B \Delta\tau \ll 1$ ), the expected trajectory and drift speed are well reproduced.

We finish our extensive test of the algorithm by considering two time varying electromagnetic field configurations represented by linearly and circularly polarized plane waves.

### 5.7. Linearly polarized plane wave

Consider a linearly polarized plane wave propagating along the  $\mathbf{e}_x$  direction such that the vector potential is  $A^\alpha = (0, 0, \frac{E}{\omega} \cos \xi, 0)$ . The wave vector is therefore  $(\frac{\omega}{c}, k, 0, 0)$  from which we deduce the phase  $\xi = \omega t - kx$ . The electromagnetic field is then given by

$$\mathbf{E} = E \sin \xi \mathbf{e}_y \quad (56a)$$

$$\mathbf{B} = \frac{E}{c} \sin \xi \mathbf{e}_z. \quad (56b)$$

Initially the particle is at rest with a 4-velocity  $u_0^\alpha = (c, \mathbf{0})$ . Introducing the strength parameter of the wave by the ratio

$$a = \frac{qE}{mc\omega} \quad (57)$$

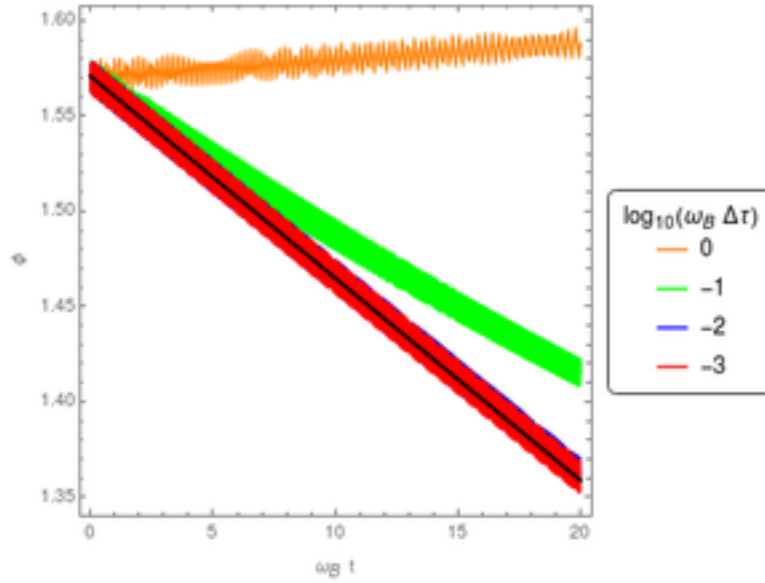


Fig. 10. Observed and expected drift speed of a positron in the equatorial plane of a magnetic dipole for  $B = 10^3$  and  $\gamma \approx 71$ .

the 4-velocity has components

$$u^x = \frac{a^2}{2} c (\cos \xi - 1)^2 \quad (58a)$$

$$u^y = -a c (\cos \xi - 1) \quad (58b)$$

$$u^0 = c + u^x. \quad (58c)$$

More generally, exact analytical solutions for plane electromagnetic waves in vacuum (linearly or circularly polarized) have been derived. The methodology using 4-vectors and tensors can be found for instance in Uzan and Deruelle (2014). See also Michel and Li (1999) for typical applications to pulsars. For brevity, we do not reproduce these computations in this work. The mean spatial velocity becomes

$$\langle v^x \rangle = \frac{3}{4} \frac{a^2 c}{1 + 3 a^2/4} \quad (59a)$$

$$\langle v^y \rangle = \frac{a c}{1 + 3 a^2/4}. \quad (59b)$$

After integration, assuming the particle starts at rest at the origin at  $\xi = 0$ , we find

$$\omega x = \frac{a^2 c}{8} (6 \xi - 8 \sin \xi + \sin 2 \xi) \quad (60a)$$

$$\omega y = a c (\xi - \sin \xi) \quad (60b)$$

$$\omega c t = c \xi + \omega x. \quad (60c)$$

The particle motion is completely described by the strength parameter  $a$  (disregarding the initial conditions that are not part of the physical parameters). Examples of motion along the  $x$  axis are shown in fig. 11 for a series of mildly and ultra-relativistic strength parameters  $a = 10^i$  with  $i \in \{0, 3, 6, 9, 12\}$ . The mean motion with average velocity  $\langle v_x \rangle$  is also shown as black solid lines. The associated Lorentz factor time evolution is shown in fig. 12. The numerical integration is compared to the analytical solution depicted by coloured symbols. Both are in perfect agreement. We are able to simulate acceleration to Lorentz factors well above  $\gamma = 10^{12}$ . This is compulsory to faithfully study lepton acceleration in neutron star magnetospheres. The true motion in this plane wave is perfectly periodic with a period given by

$$T_{\text{lin}} = 2 \pi \left( 1 + \frac{3}{4} a^2 \right) \quad (61)$$

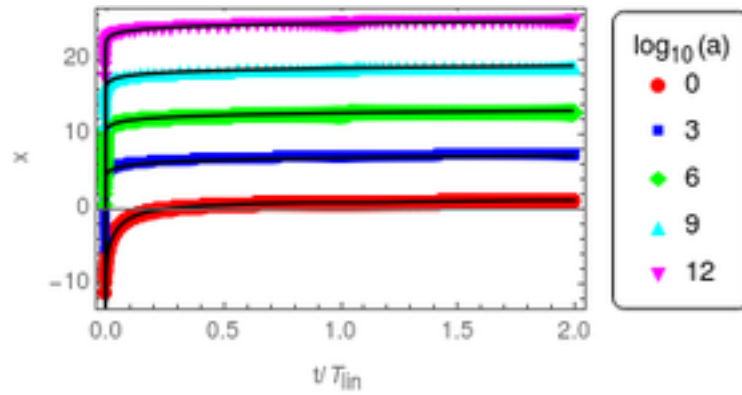


Fig. 11. Motion of an electron in a linearly polarized plane wave for different strength parameters  $a = 10^i$  with  $i \in \{0, 3, 6, 9, 12, 15, 18, 21\}$ . Symbols correspond to the analytical solution given in eq. (60).

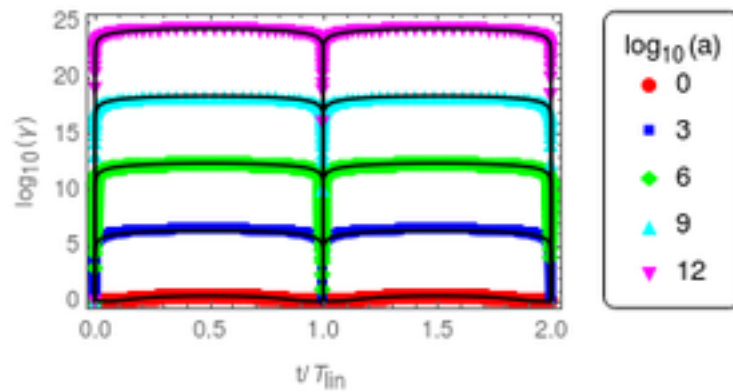


Fig. 12. Lorentz factor of an electron in a linearly polarized plane wave for different strength parameters  $a = 10^i$  with  $i \in \{0, 3, 6, 9, 12, 15, 18, 21\}$ . Symbols correspond to the analytical solution eq. (58).

the particle returning to rest at each period  $T_{\text{lin}}$ . The maximum Lorentz factor, reached at  $t = T_{\text{lin}}/2$  is

$$\gamma_{\text{max}} = 1 + 2a^2. \quad (62)$$

Arefiev et al. (2015) performed similar simulations in a strong plane electromagnetic wave and found significant discrepancies between analytical and numerical results already with strength parameters  $a \approx 25$ . Moreover the time step criterion for particle pusher they found would be too restrictive in the case of realistic pulsars or magnetars. In order to compare our results with their findings, we computed the invariant quantity (which is another expression of eq. (58c))

$$\gamma m_e c - p_x = m_e c. \quad (63)$$

We found that this invariant is well conserved for the full time of integration for any strength parameter giving always the value 1 in normalized units. We show it however in a different manner compared to Arefiev et al. (2015), instead of the above invariant, we plotted the Lorentz factors in Fig. 12. An estimate of the error is shown in fig. 15. Here also our scheme is second order in time.

### 5.8. Circularly polarized plane wave

Consider a circularly polarized plane wave propagating in the  $\mathbf{e}_x$  direction such that the vector potential has components  $A^\alpha = (0, 0, \frac{E}{\omega} \cos \xi, \frac{E}{\omega} \sin \xi)$  and the wave vector  $(\frac{\omega}{c}, k, 0, 0)$  thus the phase  $\xi = \omega t - kx$ . The electromagnetic field is then given by

$$\mathbf{E} = E (\sin \xi \mathbf{e}_y - \cos \xi \mathbf{e}_z) \quad (64a)$$

$$\mathbf{B} = \frac{E}{c} (\sin \xi \mathbf{e}_z + \cos \xi \mathbf{e}_y). \quad (64b)$$

Initially the particle is at rest with 4-velocity  $u_0^\alpha = (c, \mathbf{0})$ . The time evolution of the components of this 4-velocity will be

$$u^x = a^2 c (1 - \cos \xi) = a u^y \quad (65a)$$

$$u^y = a c (1 - \cos \xi) \quad (65b)$$

$$u^z = -a c \sin \xi \quad (65c)$$

$$u^0 = c + u^x. \quad (65d)$$

The mean spatial velocity becomes

$$\langle v^x \rangle = \frac{a^2 c}{1 + a^2} \quad (66a)$$

$$\langle v^y \rangle = \frac{a c}{1 + a^2} \quad (66b)$$

$$\langle v^z \rangle = 0. \quad (66c)$$

After integration, assuming the particle starts at rest at the origin at phase  $\xi = 0$ , we find

$$\omega x = a^2 c (\xi - \sin \xi) \quad (67a)$$

$$\omega y = a c (\xi - \sin \xi) \quad (67b)$$

$$\omega z = a c (\cos \xi - 1) \quad (67c)$$

$$\omega c t = c \xi + \omega x. \quad (67d)$$

Examples of motion along the  $x$  axis are shown in fig. 13 for mildly and ultra-relativistic strength parameters  $a = 10^i$  with  $i \in \{0, 3, 6, 9, 12\}$ . The mean motion with average velocity  $\langle v_x \rangle$  is also shown. The corresponding evolution of the Lorentz factor is given in fig. 14. The numerical integration is compared to the analytical solution depicted by coloured symbols. Here again, both are in perfect agreement. We are even able to push the Lorentz factor limit well above  $\gamma = 10^{15}$ . Circular polarization is more efficient in accelerating particles to ultra-relativistic speeds.

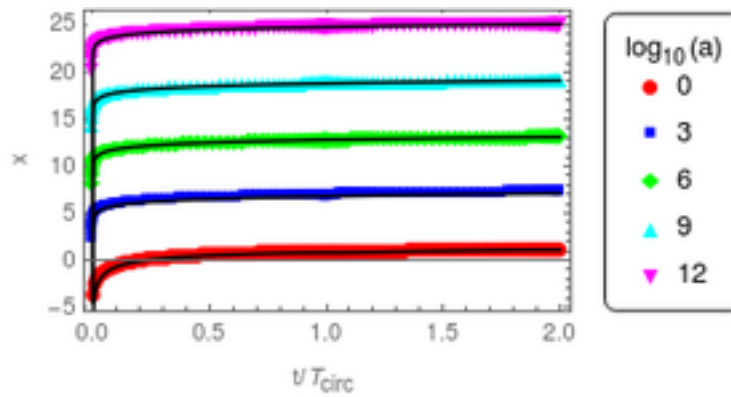


Fig. 13. Motion of a positron in a circularly polarized plane wave for different strength parameters  $a = 10^i$  with  $i \in \{0, 3, 6, 9, 12\}$ . Symbols correspond to the analytical solution eq. (67).

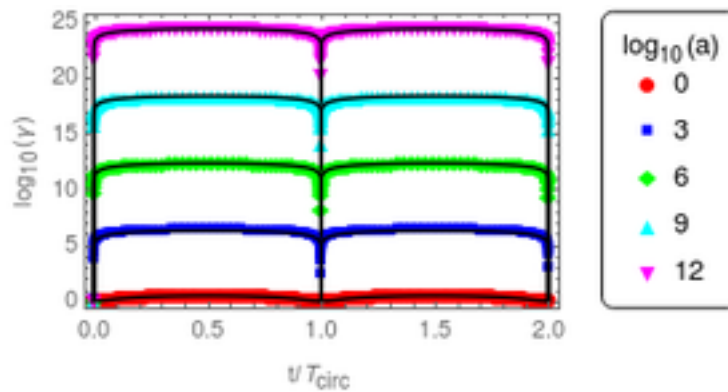


Fig. 14. Lorentz factor of a positron in a circularly polarized plane wave for different strength parameters  $a = 10^i$  with  $i \in \{0, 3, 6, 9, 12\}$ . Symbols correspond to the analytical solution eq. (65).



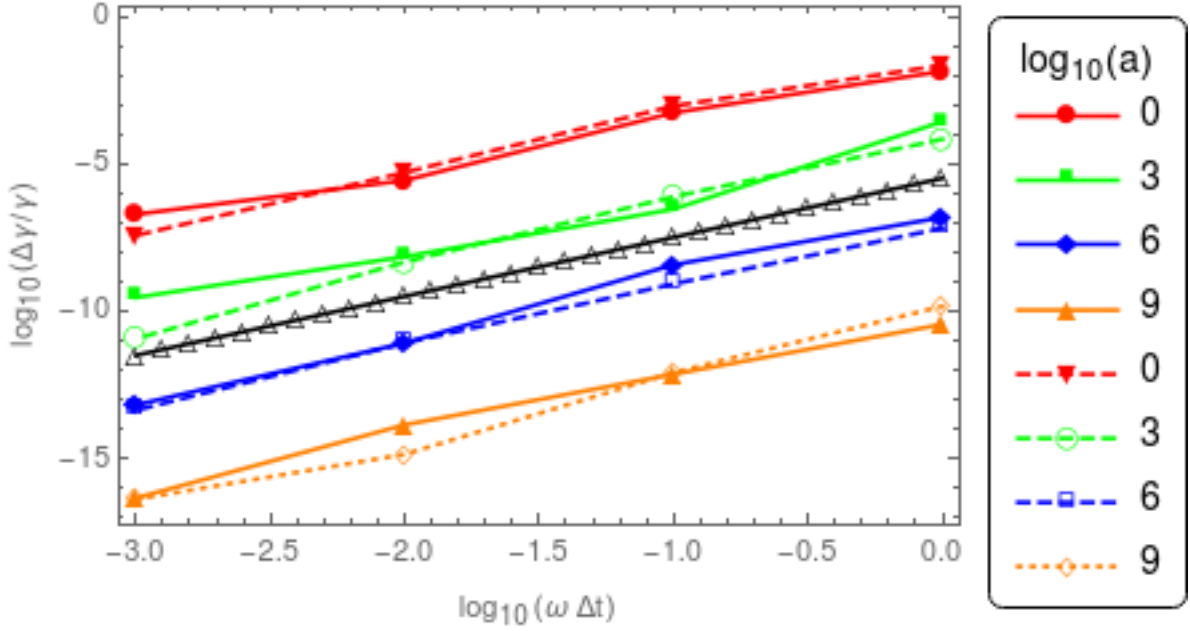


Fig. 15. Relative error  $\Delta\gamma/\gamma$  on the Lorentz factor at time  $t = T/2$  corresponding to the maximum Lorentz factor reachable, depending on observer time step  $\Delta t$  on log-log scale for the linearly, solid line, and circularly, dashed line, polarized waves and strength parameter  $a$ . The black solid line correspond to a  $\Delta t^{-2}$  slope.

The true motion in this plane wave is also perfectly periodic with a period given by

$$T_{\text{circ}} = 2\pi(1 + a^2) \tag{68}$$

the particle returning to rest at each period  $T_{\text{circ}}$ . The maximum Lorentz factor, reached at  $t = T_{\text{circ}}/2$  is the same as eq. (62). Fig. 15 again show the error in the Lorentz factor for a circularly polarized wave, second order in time still holds.

### 6. Conclusions

We designed a new scheme for particle trajectory integration in any electromagnetic field configuration by analytically solving the relativistic equation of motion for a charged particle. The trajectory is given by an explicit close analytical form free of any approximation as long as the field remains constant and uniform. For spatially and time dependent fields, numerical errors arise from these assumptions of constant fields when advancing to the next time step. Between two integration times, the motion must remains bound to size less than the typical space and time scales. These restrictions limit the size of the time step. Nevertheless, for plasmas with Larmor radii much smaller than the typical length scale of the electromagnetic field, this approximation must be excellent. It avoid resolving the gyro-period, enabling an increase by several orders of magnitude of the time step. Such approximations are particularly well suited for neutron star electromagnetic environments.

Our scheme can be seen as slicing space in small volumes of uniform electromagnetic field entities like finite volume methods (FVM) where the average quantity within one cell is advanced in time. In order to increase the order of the method, as in FVM, we could look for analytical solutions in a electromagnetic field that is linearly varying in space and or time. This should improve the spatial and temporal truncation errors as it does for FVM by reconstruction via WENO methods or using discontinuous Galerkin technique to evolve also the higher order terms instead of reconstructing. It is however not clear if such analytical solutions are tractable for linear field. Therefore we leave this possible extension for future work.

## Acknowledgements

This work has been supported by CEFIPRA grant IFC/F5904-B/2018. We also acknowledge the High Performance Computing center of the University of Strasbourg for supporting this work by providing scientific support and access to computing resources. Part of the computing resources were funded by the Equipex Equip@Meso project (Programme Investissements d'Avenir) and the CPER Alsacalcul/Big Data.

## References

- Ansoldi S, Antonelli LA, Antoranz P, Babic A, Bangale P, Almeida UBd, Barrio JA, Gonzlez JB, Bednarek W, Bernardini E, Biasuzzi B, Biland A, Blanch O, Bonnefoy S, Bonoli G, Borraici F, Bretz T, Carmona E, Carosi A, Colin P, Colombo E, Contreras JL, Cortina J, Covino S, Vela PD, Dazzi F, Angelis AD, Caneva GD, Lotto BD, Wilhelmi EdO, Mendez CD, Pierre FD, Prester DD, Dorner D, Doro M, Einecke S, Glawion DE, Elsaesser D, Fernndez-Barral A, Fidalgo D, Fonseca MV, Font L, Frantzen K, Fruck C, Galindo D, Lpez RJG, Garczarczyk M, Terrats DG, Gaug M, Godinovi N, Muoz AG, Gozzini SR, Hanabata Y, Hayashida M, Herrera J, Hirotani K, Hose J, Hrupec D, Hughes G, Idec W, Kellermann H, Knoetig ML, Kodani K, Konno Y, Krause J, Kubo H, Kushida J, Barbera AL, Lelas D, Lewandowska N, Lindfors E, Lombardi S, Longo F, Lpez M, Lpez-Coto R, Lpez-Oramas A, Lorenz E, Makariev M, Mallot K, Maneva G, Mannheim K, Maraschi L, Marcote B, Mariotti M, Martnez M, Mazin D, Menzel U, Miranda JM, Mirzoyan R, Moralejo A, Munar-Adrover P, Nakajima D, Neustroev V, Niedzwiecki A, Rosillo MN, Nilsson K, Nishijima K, Noda K, Orito R, Overkemping A, Paiano S, Palatiello M, Paneque D, Paoletti R, Paredes JM, Paredes-Fortuny X, Persic M, Poutanen J, Moroni PGP, Prandini E, Puljak I, Reinthal R, Rhode W, Rib M, Rico J, Garcia JR, Saito T, Saito K, Satalecka K, Scalzotto V, Scapin V, Schultz C, Schweizer T, Shore SN, Sillanp A, Sitarek J, Snidaric I, Sobczynska D, Stamerra A, Steinbring T, Strzys M, Takalo L, Takami H, Tavecchio F, Temnikov P, Terzi T, Tescaro D, Teshima M, Thaele J, Torres DF, Toyama T, Treves A, Ward J, Will M, Zanin R. Teraelectronvolt pulsed emission from the Crab Pulsar detected by MAGIC. *A&A* 2016;585:A133. URL: <https://www.aanda.org/articles/aa/abs/2016/01/aa26853-15/aa26853-15.html>. doi:10.1051/0004-6361/201526853.
- Arefiev AV, Cochrane GE, Schumacher DW, Robinson APL, Chen G. Temporal resolution criterion for correctly simulating relativistic electron motion in a high-intensity laser field. *Phys Plasmas* 2015;22(1):013103. URL: <http://aip.scitation.org/doi/10.1063/1.4905523>. doi:10.1063/1.4905523.
- Baumjohann W, Treumann R. *Basic Space Plasma Physics*. New edition ed. London: Imperial College Press, 1996.
- Belyaev MA. Dissipation, energy transfer, and spin-down luminosity in 2.5d PIC simulations of the pulsar magnetosphere. *Mon Not R Astron Soc* 2015;449(3):2759-67. URL: <https://academic.oup.com/mnras/article/449/3/2759/1132376>. doi:10.1093/mnras/stv468.
- Boris J. Relativistic plasma simulation-optimization of a hybrid code. *Proceeding of Fourth Conference on Numerical Simulations of Plasmas* 1970;.
- Bowers KJ, Albright BJ, Yin L, Bergen B, Kwan TJT. Ultrahigh performance three-dimensional electromagnetic relativistic kinetic plasma simulation. *Physics of Plasmas* 2008;15(5):055703. URL: <http://aip.scitation.org/doi/10.1063/1.2840133>. doi:10.1063/1.2840133.
- Cerutti B, Philippov A, Parfrey K, Spitkovsky A. Particle acceleration in axisymmetric pulsar current sheets. *MNRAS* 2015;448:606-19. URL: <http://adsabs.harvard.edu/abs/2015MNRAS.448..606C>. doi:10.1093/mnras/stv042.
- Cerutti B, Philippov AA, Spitkovsky A. Modelling high-energy pulsar light curves from first principles. *Monthly Notices of the Royal Astronomical Society* 2016;457:2401-14. URL: <http://adsabs.harvard.edu/abs/2016MNRAS.457.2401C>. doi:10.1093/mnras/stw124.
- Crouseilles N, Lemou M, Mhats F, Zhao X. Uniformly accurate Particle-in-Cell method for the long time solution of the two-dimensional Vlasov-Poisson equation with uniform strong magnetic field. *Journal of Computational Physics* 2017;346:172-90. URL: <http://www.sciencedirect.com/science/article/pii/S0021999117304564>. doi:10.1016/j.jcp.2017.06.011.
- Filbet F, Rodrigues LM. Asymptotically stable particle-in-cell methods for the Vlasov-Poisson system with a strong external magnetic field. *arXiv:151107400 [math]* 2015;URL: <http://arxiv.org/abs/1511.07400>; arXiv: 1511.07400.
- Finkbeiner B, Herold H, Ertl T, Ruder H. Effects of radiation damping on particle motion in pulsar vacuum fields. *Astronomy and Astrophysics* 1989;225:479-87. URL: <http://adsabs.harvard.edu/abs/1989A%26A...225..479F>.
- Geiser J, Riedel F. Integrators for particle in cell methods: Comparison and applications. *AIP Conference Proceedings* 2016;1738(1):480009. URL: <http://aip.scitation.org/doi/abs/10.1063/1.4952245>. doi:10.1063/1.4952245.
- Gourgoulhon E. *Relativit restreinte: Des particules l'astrophysique*. EDP Sciences, 2010.
- Gruzinov A. Aristotelian Electrodynamics solves the Pulsar: Lower Efficiency of Strong Pulsars. *arXiv:13034094 [astro-ph]* 2013;URL: <http://arxiv.org/abs/1303.4094>; arXiv: 1303.4094.
- Hadad Y, Labun L, Rafelski J, Elkina N, Klier C, Ruhl H. Effects of radiation reaction in relativistic laser acceleration. *Phys Rev D* 2010;82(9):096012. URL: <https://link.aps.org/doi/10.1103/PhysRevD.82.096012>. doi:10.1103/PhysRevD.82.096012.
- Higuera AV, Cary JR. Structure-preserving second-order integration of relativistic charged particle trajectories in electromagnetic fields. *arXiv:170105605 [physics]* 2017;URL: <http://arxiv.org/abs/1701.05605>; arXiv: 1701.05605.
- Jackson JD. *Electrodynamique classique : Cours et exercices d'electromagnitisme*. Paris: Dunod, 2001.
- Kalpatharakos C, Brambilla G, Timokhin A, Harding AK, Kazanas D. Three-dimensional Kinetic Pulsar Magnetosphere Models: Connecting to Gamma-Ray Observations. *ApJ* 2018;857(1):44. URL: <http://stacks.iop.org/0004-637X/857/i=1/a=44>. doi:10.3847/1538-4357/aab550.
- Lapenta G, Markidis S. Particle acceleration and energy conservation in particle in cell simulations. *Physics of Plasmas* (1994-present) 2011;18(7):072101. URL: <http://scitation.aip.org/content/aip/journal/pop/18/7/10.1063/1.3602216>. doi:10.1063/1.3602216.
- Mereghetti S, Pons JA, Melatos A. Magnetars: Properties, Origin and Evolution. *Space Sci Rev* 2015;191(1-4):315-38. URL: <https://link.springer.com/article/10.1007/s11214-015-0146-y>. doi:10.1007/s11214-015-0146-y.
- Michel FC, Li H. Electrodynamics of neutron stars. *Physics Reports* 1999;318(6):227-97. URL: <http://www.sciencedirect.com/science/article/pii/S0370157399000022>. doi:10.1016/S0370-1573(99)00002-2.

- Patacchini L, Hutchinson IH. Explicit time-reversible orbit integration in Particle In Cell codes with static homogeneous magnetic field. *Journal of Computational Physics* 2009;228(7):2604–15. URL: <http://www.sciencedirect.com/science/article/pii/S0021999108006608>. doi:10.1016/j.jcp.2008.12.021.
- Philippov AA, Spitkovsky A. Ab Initio pulsar magnetosphere: three-dimensional particle-in-cell simulations of axisymmetric pulsars. *The Astrophysical Journal Letters* 2014;785(2):L33. URL: <http://iopscience.iop.org/article/10.1088/2041-8205/785/2/L33/meta>. Press WH. *Numerical recipes the art of scientific computing*. Cambridge, UK; New York: Cambridge University Press, 2007. URL: <http://search.ebscohost.com/login.aspx?direct=true&scope=site&db=nlebk&db=nlabk&AN=206846>; oCLC: 748025266.
- Ptri J. Theory of pulsar magnetosphere and wind. *J Pl Ph* 2016;82(5). URL: <https://www.cambridge.org/core/journals/journal-of-plasma-physics/article/theory-of-pulsar-magnetosphere-and-wind/72D2F4DAE9EDD1D2EE5C924616D212AD>. doi:10.1017/S0022377816000763.
- Ptri J. A fully implicit numerical integration of the relativistic particle equation of motion. *J Pl Ph* 2017;83:705830206. URL: <http://cdsads.u-strasbg.fr/abs/2017JPlPh..83b7006P>. doi:10.1017/S0022377817000307.
- Ptri J. Pulsar gamma-ray emission in the radiation reaction regime. *MNRAS* 2019;484(4):5669–91. URL: <https://academic.oup.com/mnras/article/484/4/5669/5307092>. doi:10.1093/mnras/stz360.
- Qin H, Zhang S, Xiao J, Liu J, Sun Y, Tang WM. Why is Boris algorithm so good? *Physics of Plasmas* 2013;20(8):084503. URL: <http://aip.scitation.org/doi/10.1063/1.4818428>. doi:10.1063/1.4818428.
- Ripperda B, Bacchini F, Teunissen J, Xia C, Porth O, Sironi L, Lapenta G, Keppens R. A comprehensive comparison of relativistic particle integrators. arXiv:171009164 [astro-ph, physics:physics] 2017; URL: <http://arxiv.org/abs/1710.09164>; arXiv: 1710.09164.
- Sengupta P. *Classical Electrodynamics*. New Delhi: New Age International Pvt Ltd Publishers, 2007.
- Spreiter Q, Walter M. Classical Molecular Dynamics Simulation with the Velocity Verlet Algorithm at Strong External Magnetic Fields. *Journal of Computational Physics* 1999;152(1):102–19. URL: <http://www.sciencedirect.com/science/article/pii/S002199919996237X>. doi:10.1006/jcph.1999.6237.
- Umeda T. A three-step Boris integrator for Lorentz force equation of charged particles. *Computer Physics Communications* 2018;228:1–4. URL: <http://www.sciencedirect.com/science/article/pii/S0010465518300912>. doi:10.1016/j.cpc.2018.03.019.
- Uzan JP, Deruelle N. *Thories de la Relativité*. Paris: Belin, 2014.
- Vandervoort PO. The relativistic motion of a charged particle in an inhomogeneous electromagnetic field. *Annals of Physics* 1960;10(3):401–53. URL: <http://www.sciencedirect.com/science/article/pii/000349166090004X>. doi:10.1016/0003-4916(60)90004-X.
- Vay JL. Simulation of beams or plasmas crossing at relativistic velocity. *Physics of Plasmas* (1994-present) 2008;15(5):056701. URL: <http://scitation.aip.org/content/aip/journal/pop/15/5/10.1063/1.2837054>. doi:10.1063/1.2837054.
- Verboncoeur JP. Particle simulation of plasmas: review and advances. *Plasma Phys Control Fusion* 2005;47(5A):A231. URL: <http://stacks.iop.org/0741-3335/47/i=5A/a=017>. doi:10.1088/0741-3335/47/5A/017.
- Vranic M, Martins JL, Fonseca RA, Silva LO. Classical radiation reaction in particle-in-cell simulations. *Computer Physics Communications* 2016;204:141–51. URL: <http://www.sciencedirect.com/science/article/pii/S001046551630090X>. doi:10.1016/j.cpc.2016.04.002.
- Zenitani S, Umeda T. On the Boris solver in particle-in-cell simulation. arXiv:180904378 [physics] 2018; URL: <http://arxiv.org/abs/1809.04378>; arXiv: 1809.04378.
- Zhang R, Liu J, Qin H, Wang Y, He Y, Sun Y. Volume-preserving algorithm for secular relativistic dynamics of charged particles. *Physics of Plasmas* 2015;22(4):044501. URL: <https://aip.scitation.org/doi/10.1063/1.4916570>. doi:10.1063/1.4916570.